Electronic Supplementary Information for

Formalizing structure-property relationships of highly-oxidizing and weakly-reducing organic cyanoarene photocatalysts

Brandon M. Hosford,[a] Mik Patel,[a] Rolando Calderón-Oliver, [a] Maren B. Thompson,[a] Jennifer S. Cortez,[a] and Jessica R. Lamb*[a]

[a]*Department of Chemistry, University of Minnesota—Twin Cities, 207 Pleasant Street SE, Minneapolis, MN 55455, United States*

*Corresponding author. Email: jrlamb@umn.edu

Table of Contents

I. General information

A. Instrumentation and methods

Cyclic voltammetry experiments were conducted in an MBraun glovebox under an atmosphere of purified nitrogen. Measurements were collected using a WaveNowXV Potentiostat and Aftermath software package (Pine Research). A three-electrode electrochemical cell consisting of a 3 mm glassy carbon disk working electrode (CH instruments), platinum wire counter electrode (CH instruments), and a low-profile non-aqueous silver wire reference electrode (Pine Research) was used. The working electrode was polished using an alumina and water slurry (0.05 μm particle size BASi Research Products), washed with methanol, and allowed to dry. Similarly, the silver wire of the reference electrode was polished with sandpaper (600 grit), washed with methanol, and dried. The reference electrode was assembled inside the glovebox. Analyte solutions were prepared with dry, degassed MeCN and tetrabutylammonium tetrafluoroborate (Sigma Aldrich) as the supporting electrolyte (100 mM in MeCN). The electrochemical cell was filled up halfway with analyte solution, the electrodes were submerged, and the bottoms were aligned to the same depth. The working electrode potentials were referenced against the ferrocene redox couple. Potentials were converted from referencing against ferrocene to saturated calomel electrode (SCE) by adding 0.38 V.[1]

Emission measurements were performed on an Agilent Cary Eclipse spectrophotometer in 1 cm quartz cuvettes using MeCN as the solvent in the indicated concentrations.

Gas chromatography measurements were taken on a Shimadzu GC-2010 System with an FID, an SH-Rxi-5ms (0.25 mm ID) column, and helium (Airgas, UHP grade) used as the carrier gas. Method parameters: split injection (1.0 μL injection volume), column flow rate of 2.43 mL/min, and the following temperature profile: 50 °C for 3 min, increase by 10 °C/min until 280 °C, hold for 3 min. Quantitative GC analysis was performed by adding the internal standard 1-bromonaphthalene to the reaction mixture.

NMR spectra were recorded on a Bruker 500 MHz Avance III HD instrument with a Prodigy TCI cryoprobe [(^{1}H, 500 MHz)] with shifts reported relative to the residual solvent peak [$CDCl_3$: 7.26 ppm (^{1}H), acetone-d_6: 2.05 ppm (^{1}H)] or a Bruker 600 MHz Avance NEO instrument with a triple resonance cryoprobe [(^{1}H, 600 MHz), (^{13}C, 151 MHz), (^{19}F, 564 MHz)]. Data are reported as follows: chemical shift, multiplicity (s = singlet, d = doublet, t = triplet, q = quartet, m =

multiplet), coupling constants (in Hz), and integration. Deuterated chloroform and acetone were purchased from Cambridge Isotope Laboratories. Structural assignments were made with additional information from ^{19}F–^{13}C HMQCGP experiments.

Photochemical reactions were performed using a Kessil PR160L 50W 456 nm lamp at 100% power placed in an EvoluChem PhotoRedOx Box. The box is placed on top of a magnetic stirrer inside of a fume hood. See Section SIII.B for more details.

Size-exclusion chromatography (SEC) analyses for polymers were performed on a Waters Arc HPLC with three Agilent PL-Gel Mixed C columns (diameter: 7.5 mm, length: 30 cm, particle size: 5 μm polystyrene-divinylbenzene matrix) with Wyatt Optilab dRI detector with a flow rate of 1 mL/min with THF as the eluent. The SEC was calibrated with Agilent EasiCalPS poly(styrene) (PS) standards (364–1.18 kDa) in the same solvent. Samples were filtered through 0.2 μm poly(tetrafluoroethylene) (PTFE) syringe filters.

Solvent purification system was purchased from Pure Process Technology (PPT) and features two packed columns of neutral alumina for each solvent. Argon is used as the inert gas. Solvents were sparged to degas prior to loading onto the columns.

Time-correlated single-photon counting (TCSPC) measurements were taken using a PicoQuant LDH-P-C-375 laser diode, a PicoQuant PDL 800-B driver, a Horiba Jobin Yvon H-10 D UV monochromator, a Micro Photon Devices PDM series detector, and a PicoQuant TimeHarp 200 processor. Measurements were taken in front face geometry, and photon count rates were at <1% of the laser repetition rate. Measurements taken at a 2.5 MHz repetition rate to obtain the nanosecond prompt fluorescence lifetimes had a ~0.3 mW, 375 nm excitation. Samples were in ambient atmosphere. Measurements taken at a 50 kHz repetition rate (by externally triggering the PDL 800-B driver with an SRS DG535) to obtain the microsecond delayed fluorescence lifetimes had a ~6 μW, 375 nm excitation. Samples were sparged with argon for 30 seconds before measuring to eliminate quenching by O_2. All samples had 0.5-1.5 OD and were prepared in MeCN and filtered through a 0.2 μm PTFE syringe filter into a 1 cm screw-cap quartz cuvette. The instrument response function (IRF) of the TCSPC measurements was taken with coffee creamer as a highly scattering sample. Fitting was performed by convoluting the IRF with a sequential first-order kinetic model, where each state has an amplitude of A_1, A_2, and A_3, time-dependent weights of states A, B, and C were normalized to 1, and A_3 was fixed at 0. Fitting performed with a single first-order process was insufficient to capture the dynamics.

$$A_1 \xrightarrow{\frac{1}{\tau_1}} A_2 \xrightarrow{\frac{1}{\tau_2}} A_3$$

Samples of 0.5–1.0 OD were prepared in MeCN and were filtered using a 0.2 μm PTFE syringe filter before being placed into a 1 cm screw-cap quartz cuvette and sparged with argon for 30 seconds prior to measuring to eliminate quenching by O_2.

Ultraviolet and visible (**UV-Vis)** light absorbance measurements were performed on a Varian Cary 4000 spectrophotometer using a deuterium arc lamp (for UV range,190–350 nm) and

tungsten halogen lamp (for visible range, 330–1100 nm) with a silicon photodiode detector. 1 cm quartz cuvettes were used for measurements of solutions in MeCN at the indicated concentrations so that all peaks of interest measure below an absorbance of 1, unless specified otherwise.

NMR analyses were performed at the UMN Department of Chemistry Nuclear Magnetic Resonance Laboratory, supported by the Research and Innovation Office (RIO), College of Science and Engineering (CSE), the Department of Chemistry at UMN, and the Office of the Director, National Institutes of Health (NIH, S10OD011952). Part of this work was carried out in the CSE Polymer Processing and Characterization Facility at UMN, which has received capital equipment funding from the NSF through the UMN MRSEC. X-ray diffraction analysis was performed using a crystal diffractometer acquired through an NSFMRI award (CHE-1229400) in the X-ray laboratory at the University of Minnesota (UMN) supervised by Dr. Victor G. Young, Jr. The content of this paper is the sole responsibility of the authors and does not represent the official views of or endorsement by the NSF or NIH**.**

B. Sources of solvents and reagents

Acetone was purchased from Sigma Aldrich and used as received.

Acetonitrile (MeCN) was purchased from Sigma Aldrich and used as received.

Bisphenol A was purchased from Fisher Scientific and used as received.

2,7-Bis(trifluoromethyl)carbazole was purchased from Chem Scene and used as received.

3,6-Bis(trifluoromethyl)carbazole was synthesized according to previous literature.[2]

Cl-4CzIPN was synthesized according to previous literature[3] (See Section IV.A).

2,4,6-Collidine was purchased from Sigma Aldrich and used as received.

3,6-Dichlorocarbazole was synthesized according to previous literature.[4]

Dichloromethane (DCM) was purchased from Sigma Aldrich and used as received.

2-Dicyclohexylphosphino-2′,4′,6′-triisopropylbiphenyl (XPhos) was purchased from Oakwood Chemical and stored in a glovebox prior to use.

Diethyl ether, anhydrous (Et_2O) was purchased from Thermo Fisher Scientific and used as received.

3,4-Difluorothiolphenol was purchased from Oakwood Chemical and used as received.

Dimethoxy bisphenol A was synthesized according to previous literature.[5]

Ethyl acetate (EtOAc) was purchased from Sigma Aldrich and used as received.

Ferrocene was purchased from Sigma Aldrich and stored in a glovebox prior to use.

Hexanes was purchased from Sigma Aldrich used as received.

4-Iodobenzotrifluoride was purchased from Oakwood Chemical and used as received.

Iodomethane was purchased from Sigma Aldrich and used as received.

Methanol, anhydrous (MeOH) was purchased from Sigma Aldrich and used as received.

***N*,*N*-Dimethylformamide (DMF)** was purchased from Thermo Fisher Scientific and used as received.

Palladium(II) acetate was purchased from Strem Chemicals and used as received.

Pivalic Acid (PivOH) was purchased from Oakwood Chemical and used as received.

Poly(Bisphenol A-*co*-epichlorohydrin) (Phenoxy Resin) was purchased from Scientific Polymer Products and used as received.

Potassium carbonate was purchased from Fisher Scientific and used as received.

Sodium hydride (90%) was purchased from Sigma Aldrich and stored in a glovebox and used as received.

Sodium sulfate, anhydrous was purchased from Thermo Fisher Scientific and used as received.

Tetrabutylammonium tetrafluoroborate ($Bu_4N^+BF_4^-$) was purchased from Thermo Fisher, dried in a Fisherbrand Isotemp Model 281A Vacuum Oven at 80 ºC overnight equipped with an external trap attached to a Welch 1402B-01 DuoSeal vacuum pump before being stored in a glovebox.

Tetrachloroisophthalonitrile was purchased from TCI and used as received.

Tetrafluoroisophthalonitrile was purchased from TCI and used as received.

Tetrahydrofuran (THF) was purchased from Sigma Aldrich and used as received.

Toluene, anhydrous was purchased from Sigma Aldrich and used as received.

4-(Trifluoromethyl)aniline was purchased from Oakwood Chemical and used as received.

II. Supplemental data

A. Steady-state absorbance spectra

The following absorbance spectra were taken with the solutions of each PC in MeCN used for TCPSC. Samples were filtered through a 0.2 μm PTFE syringe filter to eliminate scattering of any solids and were sparged with argon. The spectra were normalized to account for differences in solubility and photophysical properties of each sample.

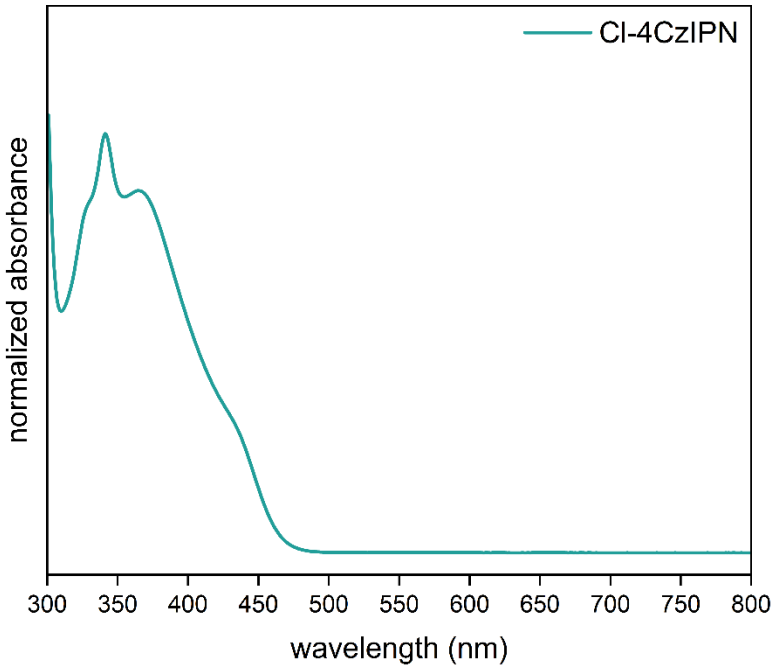

Figure S1. Steady-state absorption spectrum of Cl-4CzIPN (63 µM) normalized to the point of maximum absorbance. Sample was sparged with argon.

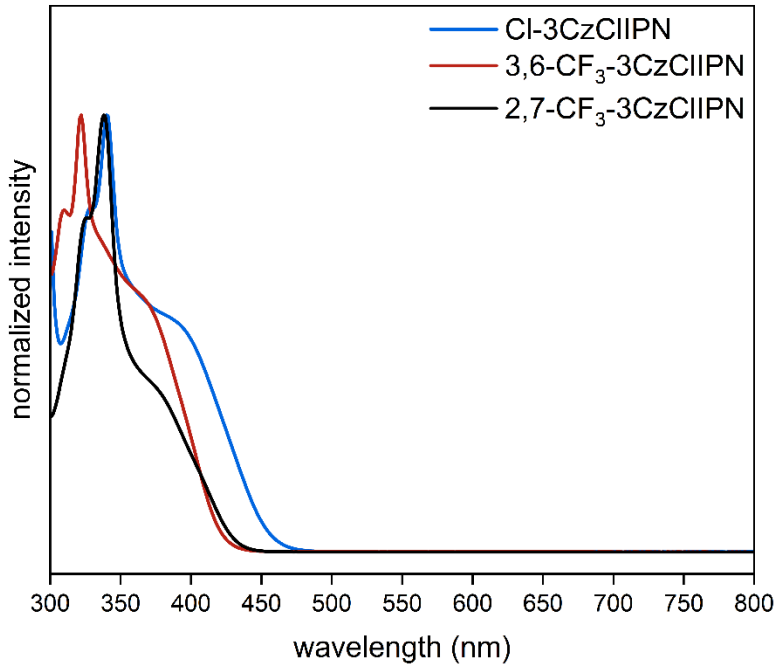

Figure S2. Combined steady-state absorption spectra of Cl-3CzClIPN (blue, 3.14x dilution from saturated), 3,6-CF_3-3CzClIPN (red, 53 µM), and 2,7-CF_3-3CzClIPN (black, 127 µM), normalized to the point of maximum absorbance. Samples were sparged with argon.

B. Steady-state emission spectra

The following emission spectra were taken with the solutions of each PC in MeCN used for TCPSC. Samples were filtered through a 0.2 µm PTFE syringe filter to eliminate scattering of any solids and were sparged with argon. The spectra were normalized to account for differences in solubility and photophysical properties of each sample.

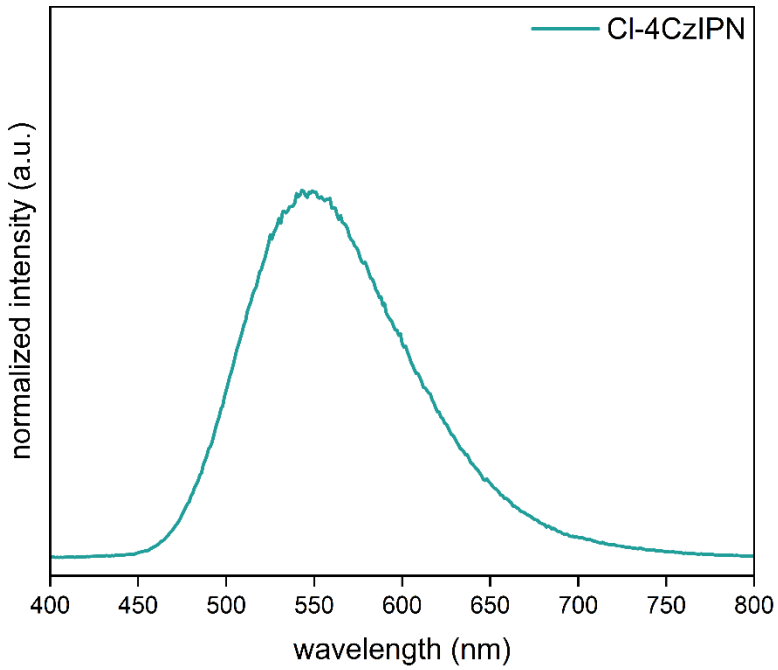

Figure S3. Steady-state emission spectrum of Cl-4CzIPN (63 µM) normalized to the point of maximum intensity. Sample was sparged with argon. Excitation wavelength = 375 nm.

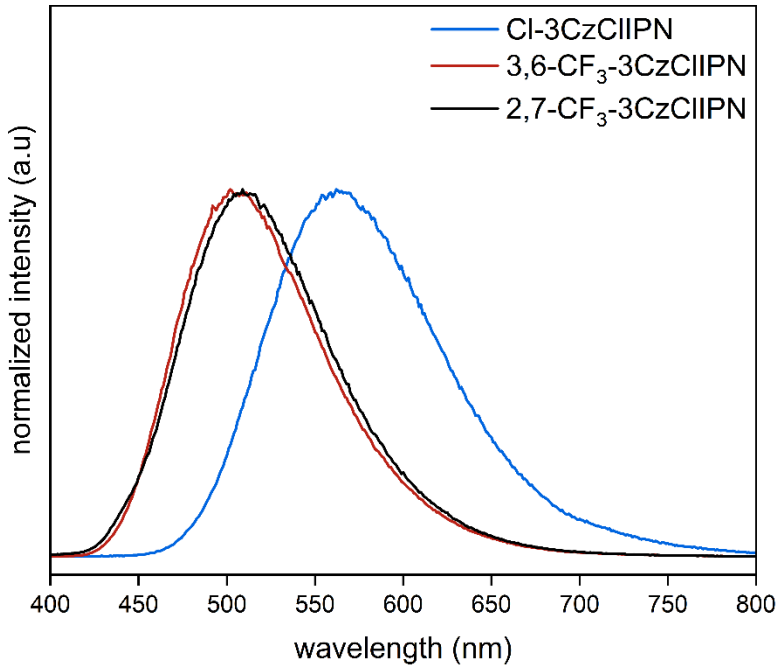

Figure S4. Combined steady-state emission spectra of Cl-3CzClIPN (blue, 3.14x dilution from saturated), 3,6-CF_3-3CzClIPN (red, 53 µM), and 2,7-CF_3-3CzClIPN (black, 127 µM), normalized to the point of maximum intensity. Samples were sparged with argon. Excitation wavelength = 375 nm for all PCs.

There is an obvious blue-shift in emission for the CF_3-containing PCs compared to Cl-3CzClIPN. This effect was previously reported with 3,6-CF_3-4CzIPN and 2,7-CF_3-4CzIPN[6] and is attributed to the more withdrawing CF_3-functionalized carbazoles lowering the HOMO of the PC, increasing the HOMO-LUMO energy gap.

C. Determination of zero-zero excitation energy

The energy between the ground state and the lowest excited electronic state (E_{0-0}) is estimated by the energy of the intersection between the normalized absorbance and emission spectra. The point of normalization for the absorbance spectrum is the estimated peak maximum of the lowest energy feature of the absorbance spectrum, which is estimated to correspond to the $S_0 \rightarrow S_1$ transition. Previous reports of similar cyanoarene PCs[2,3,7,8] have used the same feature in the absorbance plot, but it should be noted that these are estimations with inherent error. The emission spectrum is normalized to the point of maximum emission.

We compare the E_{0-0} values of the newly synthesized 3CzCl PCs with their 4Cz counterparts. The literature value for Cl-4CzIPN[3] was mistakenly normalized to the global maximum and not to the approximate $S_0 \rightarrow S_1$ transition, changing the crossover wavelength, and so we remeasured the absorbance and emission spectra using our method in order to make the comparison more consistent.

Cl-3CzClIPN, 3,6-CF_3-3CzClIPN, and 2,7-CF_3-3CzClIPN have E_{0-0} values of 2.66 eV, 2.89 eV, and 2.85 eV, respectively. With visible light irradiation (> 400 nm), the theoretical maximum E_{0-0}

is ~3.0 eV, which indicates the CF_3-containing cyanoarene PCs have minimal energy losses from thermalization processes when converting light into chemical potential.

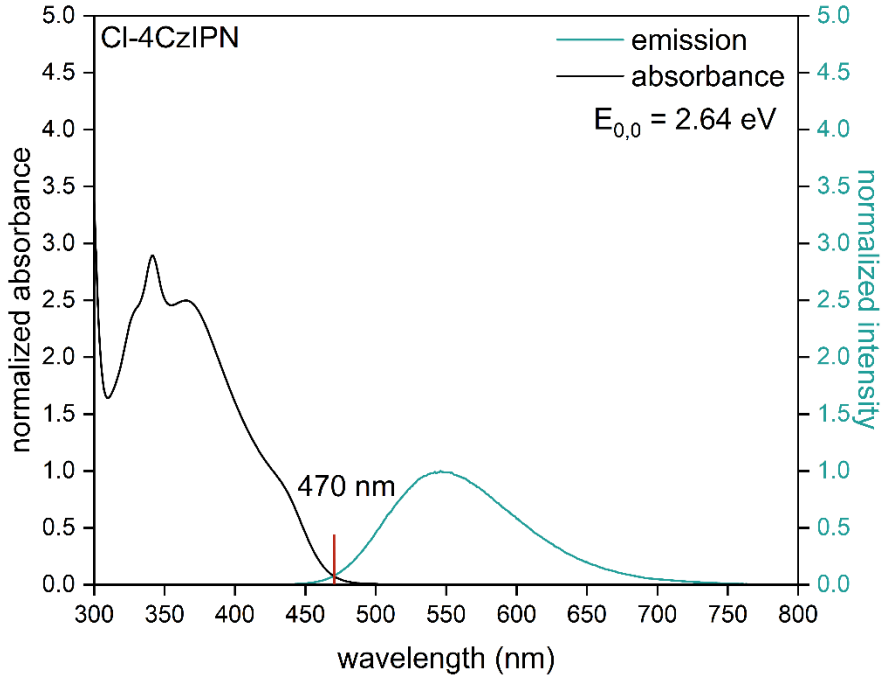

Figure S5. Normalized absorbance and emission spectra of Cl-4CzIPN. Taken at 5 µM in acetonitrile.

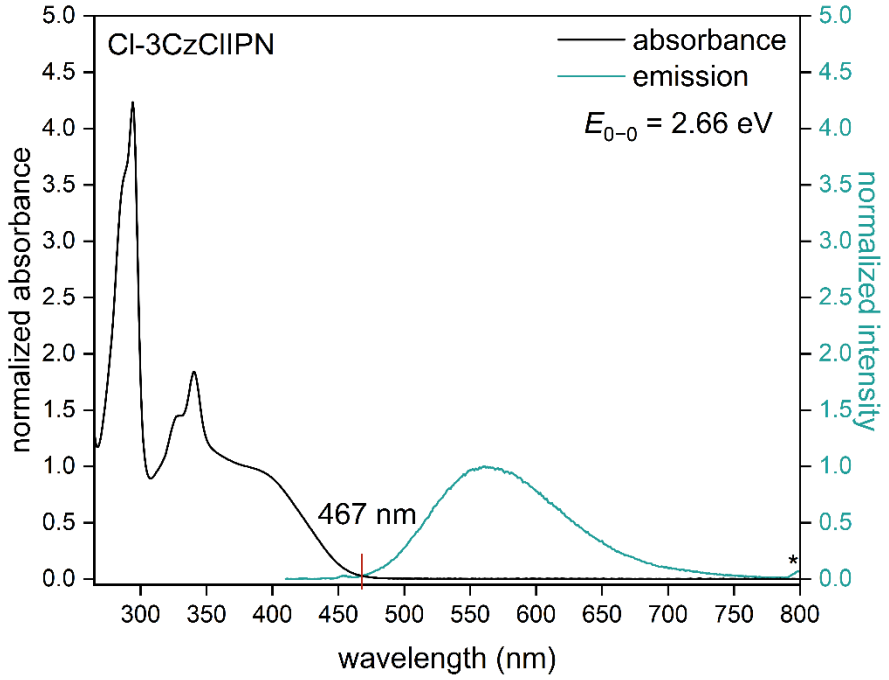

Figure S6. Normalized absorbance and emission spectra of Cl-3CzClIPN. Taken at 50 µM in MeCN. Excitation wavelength: 400 nm. *Raman scattering peak (see Section SII.C.1 for details).

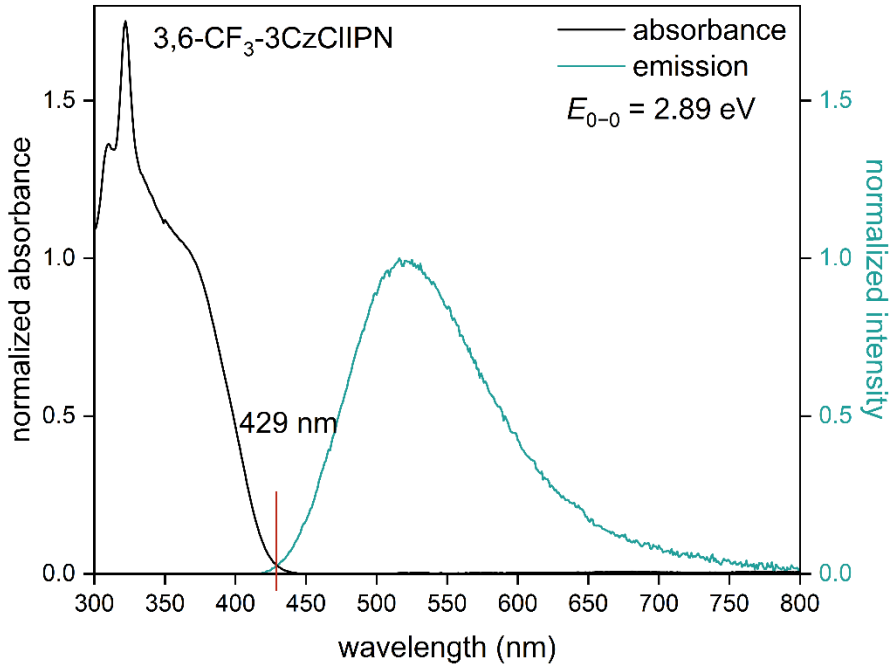

Figure S7. Normalized absorbance and emission spectra of 3,6-CF_3-3CzClIPN. Taken at 5 µM in acetonitrile. Excitation wavelength: 400 nm.

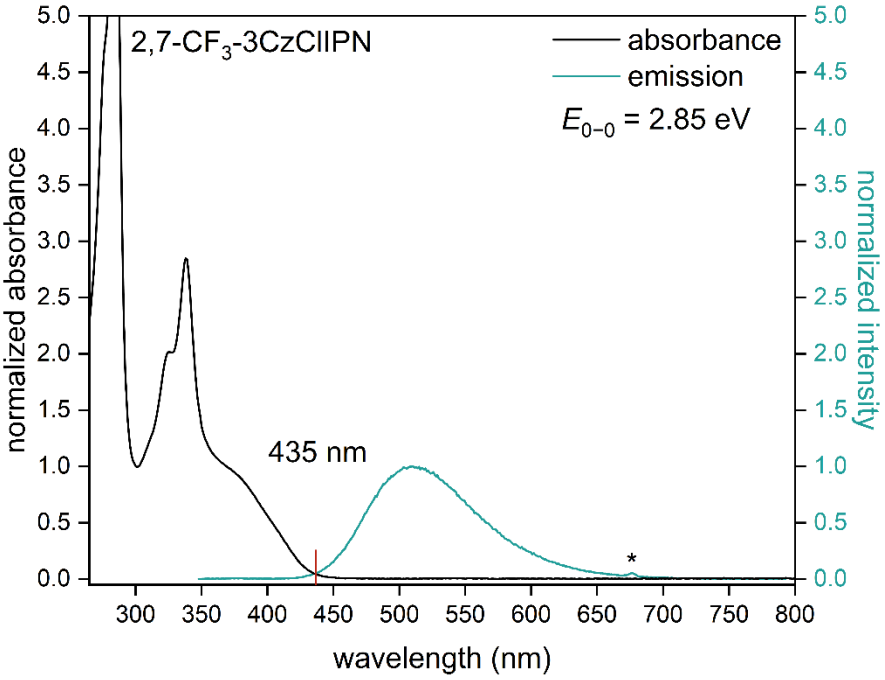

Figure S8. Normalized absorbance and emission spectra of 2,7-CF_3-3CzClIPN. Taken at 5 µM in acetonitrile. Excitation wavelength: 338 nm. *Raman scattering peak (see Section SII.C.1 for details).

1. Investigation into Raman scattering peaks seen in the emission spectra

In the emission spectra of Cl-3CzClIPN (Figure S6) and 2,7-CF_3-3CzClIPN (Figure S8), a small peak past 650 nm was observed. We believe this peak was not a result of emission from the PC sample, but is instead Raman scattering from the MeCN. To validate this hypothesis, emission spectra of an MeCN blank (Figure S9) were taken at three different excitation wavelengths (350 nm, 375nm, and 400 nm). A single peak was observed, which shifted to longer wavelengths as the excitation wavelength was increased. This is a well-reported phenomenon symptomatic of Raman scattering.[9]

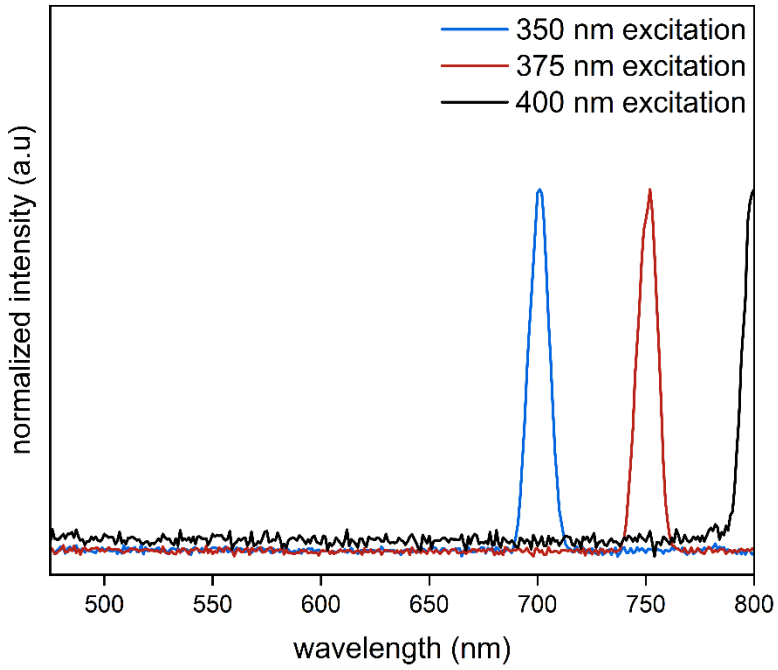

Figure S9. Raman scattering in emission measurements of MeCN at varying excitation wavelengths.

D. Time-correlated single-photon counting (TCSPC) lifetime measurements

Measurement of prompt lifetimes (τ_1) was performed using a repetition rate of 2.5 MHz with solutions in air. Measurement of the much slower delayed fluorescence lifetimes (τ_2) was performed using a repetition rate of 50 kHz with argon sparged samples.[10] The fitting parameters of both sets of measurements is found below (Table S1 and Table S2).

The delayed lifetime of Cl-4CzIPN had been previously acquired in toluene.[43] We reacquired both lifetimes in MeCN for comparison with the other PCs in the study.

Table S1. Fit parameters for 2.5 MHz TCSPC measurements. τ_2 not reliable under these conditions due to high repetition frequency

entry	photocatalyst	τ_1 (ns)[d]	τ_2 (ns)	A_1	A_2	MSR
1	Cl-4CzIPN	10.22±0.02	142±4	1.098±0.001	0.0198±0.0004	16×10^{-6}
2	Cl-3CzClIPN	5.88±0.01	127±2	1.198±0.001	0.0202±0.0003	9×10^{-6}
3	3,6-CF_3-3CzClIPN	10.74±0.02	169±4	1.100±0.001	0.0238±0.0004	23×10^{-6}
4	2,7-CF_3-3CzClIPN	11.34±0.02	181±5	1.066±0.001	0.0240±0.0005	29×10^{-6}

All measurements taken in MeCN in air to minimize delayed lifetimes. τ_1 = prompt fluorescence lifetime, τ_2 = delayed fluorescence lifetime, A_1 = amplitude of prompt decay, A_2 = amplitude of delayed decay, MSR = mean squared residuals. A_3 is 0 for all entries (fixed during fitting optimization). Error reported as 1 standard deviation from a nonlinear least-squares fit.

Table S2. Fit parameters for 50 kHz TCSPC measurements. τ_1 not reliable under these conditions due to long instrument response caused by low repetition frequency

entry	photocatalyst	τ_1 (ns)[d]	τ_2 (ns)	A_1	A_2	MSR
1	Cl-4CzIPN	10.22±0.02	620±10	2.082±0.003	0.0223±0.0003	8×10^{-6}
2	Cl-3CzClIPN	6.44±0.01	270±4	2.555±0.004	0.0310±0.0004	7×10^{-6}
3	3,6-CF_3-3CzClIPN	15.20±0.02	2800±20	1.911±0.002	0.0328±0.0001	6×10^{-6}
4	2,7-CF_3-3CzClIPN	15.22±0.04	2300±30	1.842±0.003	0.0325±0.0002	18×10^{-6}

All measurements taken in MeCN in argon. τ_1 = prompt fluorescence lifetime, τ_2 = delayed fluorescence lifetime, A_1 = amplitude of prompt decay, A_2 = amplitude of delayed decay, MSR = mean squared residuals. A_3 is 0 for all entries (fixed during fitting optimization). Error reported as 1 standard deviation from a nonlinear least-squares fit.

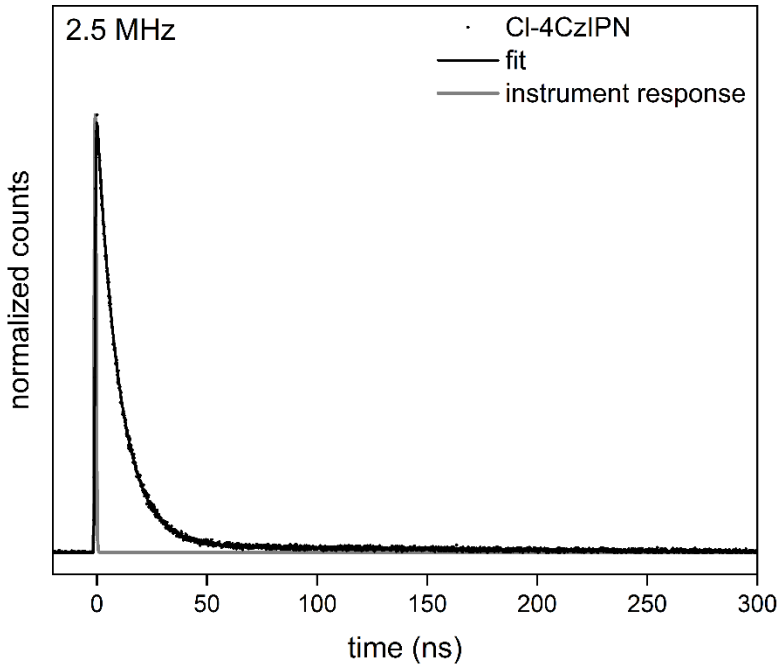

Figure S10. 2.5 MHz TCSPC measurement of Cl-4CzIPN in MeCN (63 µM), excited at 375 nm and detected at 550 nm. Raw data (black points) were fit (black line) to a sequential first-order kinetic model convoluted with the instrument response (gray line).

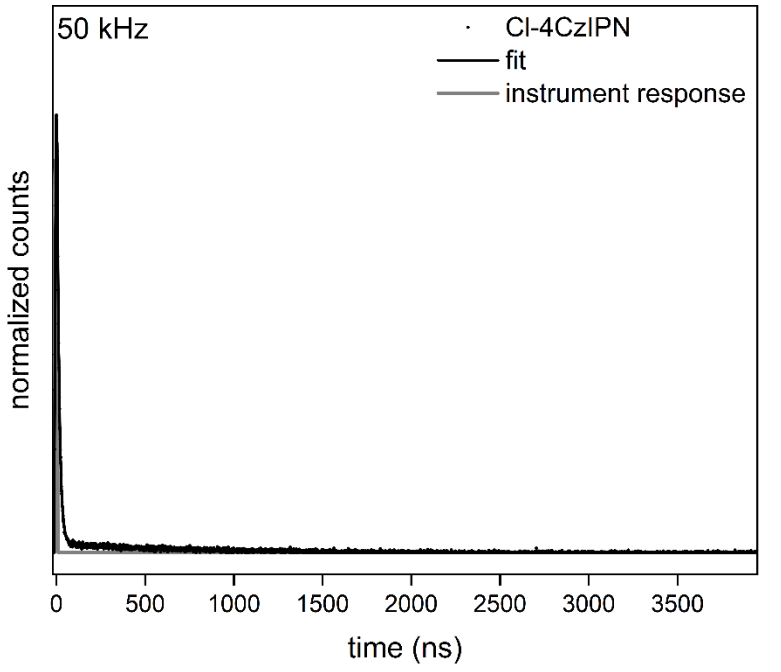

Figure S11. 50 kHz TCSPC measurement of argon-sparged Cl-4CzIPN in MeCN (63 µM), excited at 375 nm and detected at 550 nm. Raw data (black points) were fit (black line) to a sequential first-order kinetic model convoluted with the instrument response (gray line).

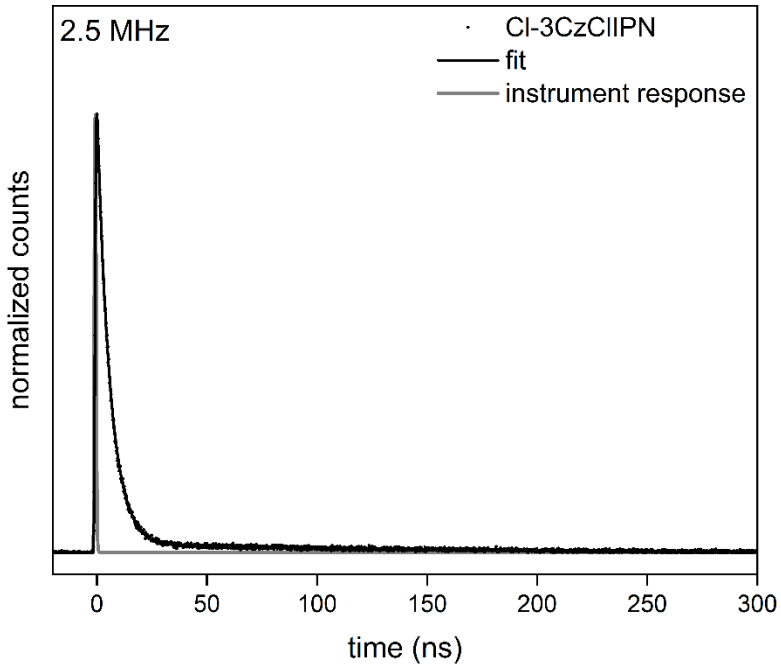

Figure S12. 2.5 MHz TCSPC measurement of Cl-3CzClIPN in MeCN (3.14x dilution from saturated), excited at 375 nm and detected at 560 nm. Raw data (black points) were fit (black line) to a sequential first-order kinetic model convoluted with the instrument response (gray line).

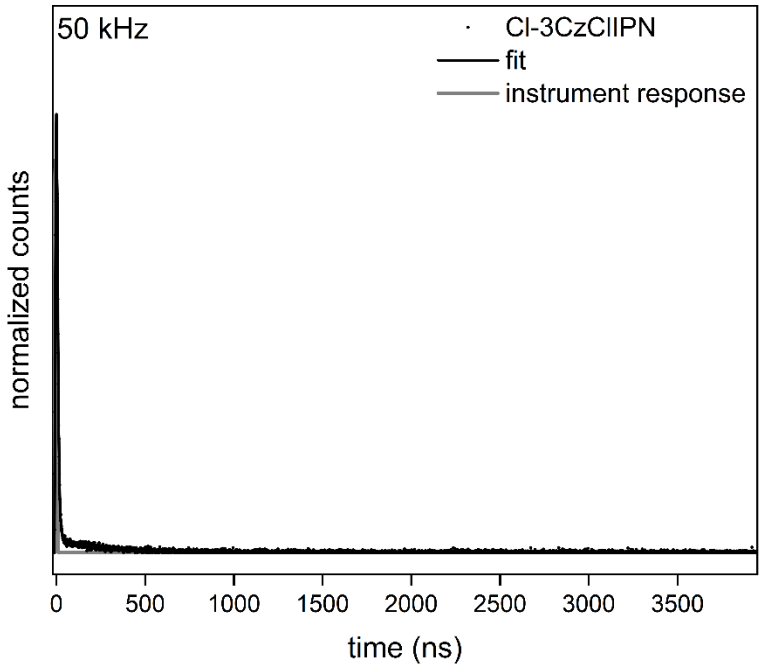

Figure S13. 50 kHz TCSPC measurement of Cl-3CzClIPN in MeCN (3.14x dilution from saturated), excited at 375 nm and detected at 560 nm. Raw data (black points) were fit (black line) to a sequential first-order kinetic model convoluted with the instrument response (gray line).

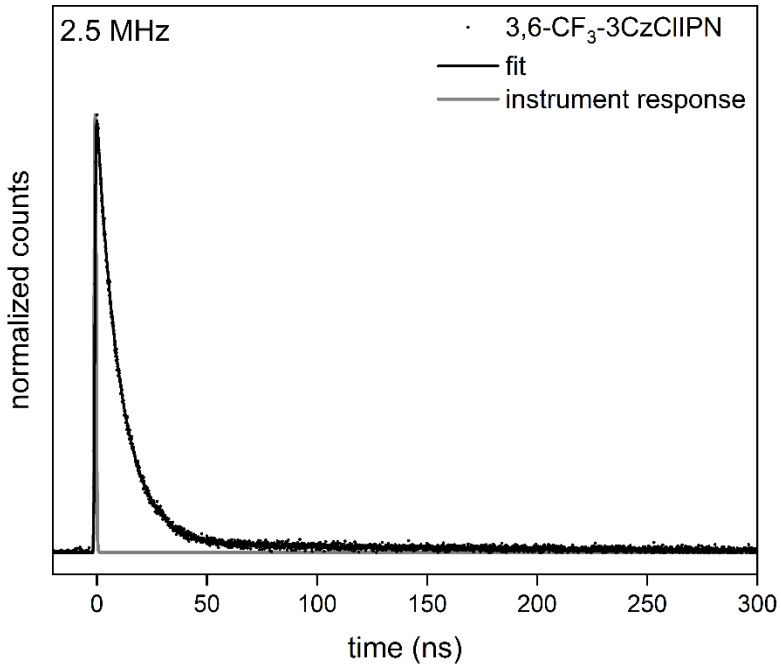

Figure S14. 2.5 MHz TCSPC measurement of 3,6-CF_3-3CzClIPN in MeCN (53 µM), excited at 375 nm and detected at 505 nm. Raw data (black points) were fit (black line) to a sequential first-order kinetic model convoluted with the instrument response (gray line).

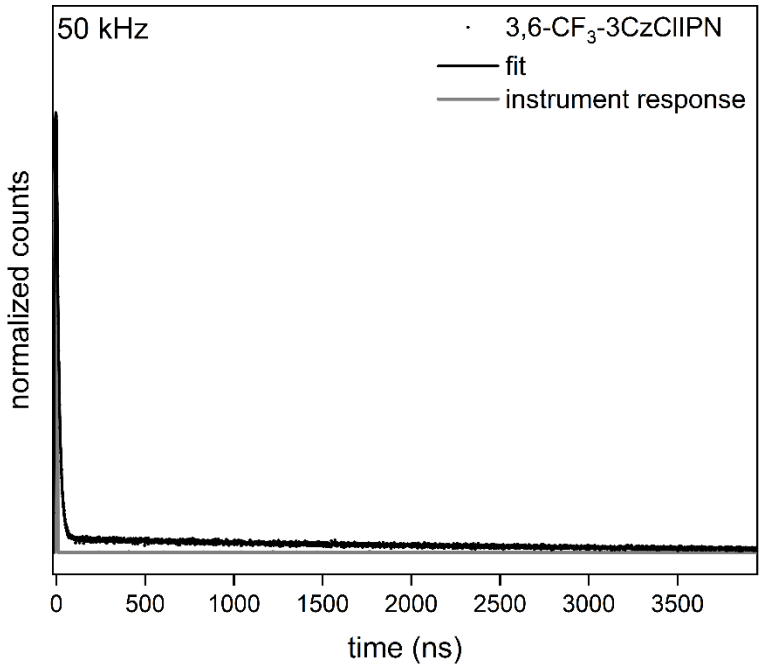

Figure S15. 50 kHz TCSPC measurement of 3,6-CF_3-3CzClIPN in MeCN (53 µM), excited at 375 nm and detected at 505 nm. Raw data (black points) were fit (black line) to a sequential first-order kinetic model convoluted with the instrument response (gray line).

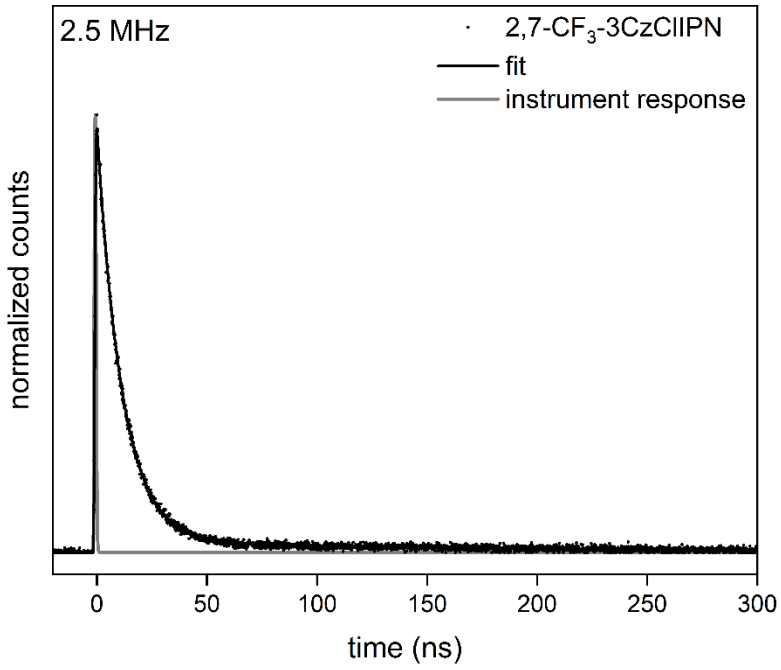

Figure S16. 2.5 MHz TCSPC measurement of 2,7-CF_3-3CzClIPN in MeCN (127 µM), excited at 375 nm and detected at 510 nm. Raw data (black points) were fit (black line) to a sequential first-order kinetic model convoluted with the instrument response (gray line).

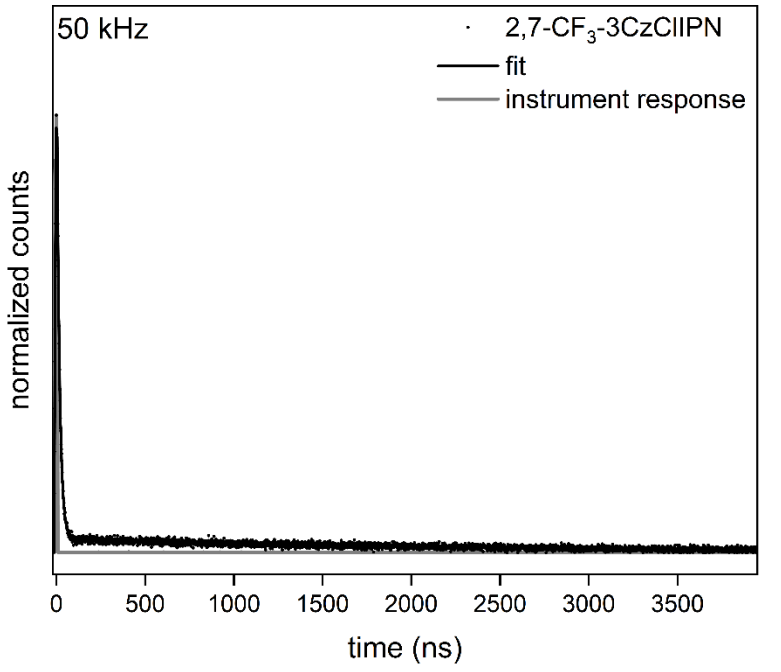

Figure S17. 50 kHz TCSPC measurement of 2,7-CF_3-3CzClIPN in MeCN (127 µM), excited at 375 nm and detected at 510 nm. Raw data (black points) were fit (black line) to a sequential first-order kinetic model convoluted with the instrument response (gray line).

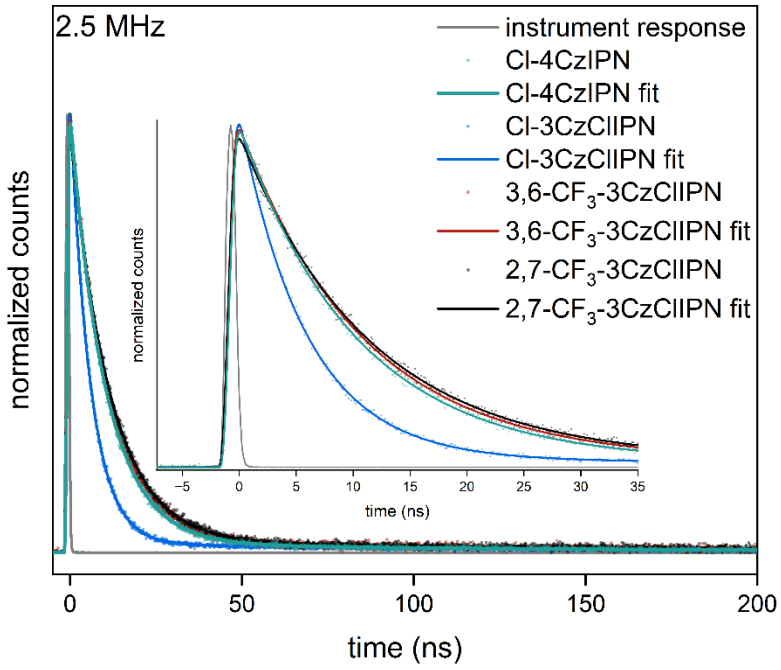

Figure S18. Combined 2.5 MHz TCSPC decay traces (points) of Cl-4CzIPN (green), Cl-3CzClIPN (blue), 3,6-CF_3-3CzClIPN (red), and 2,7-CF_3-3CzClIPN (black) with the corresponding fit (line) and instrument response (gray line).

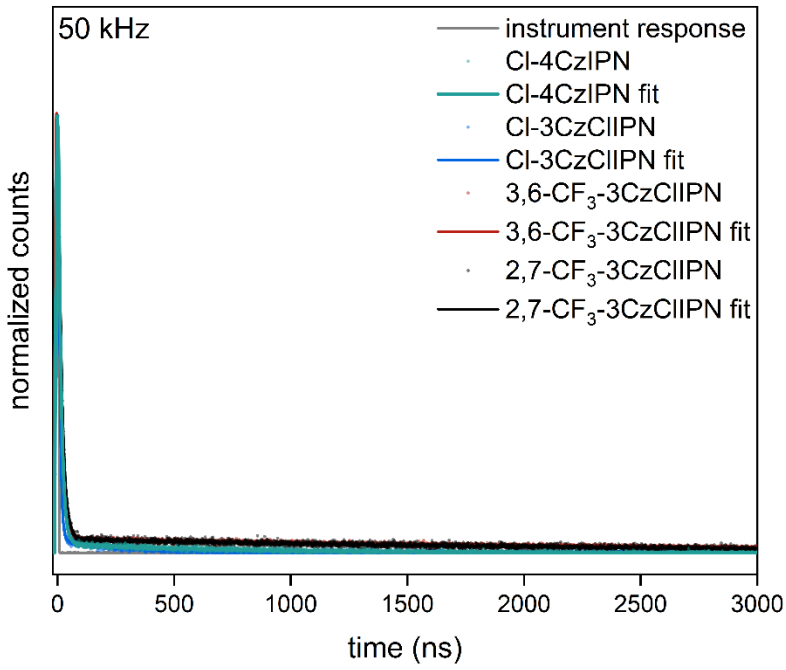

Figure S19. Combined 50 kHz TCSPC decay traces (points) of Cl-4CzIPN (green), Cl-3CzClIPN (blue), 3,6-CF_3-3CzClIPN (red), and 2,7-CF_3-3CzClIPN (black) with the corresponding fit (line) and instrument response (gray line). Full plot (for zoomed in plots, see Figure S20).

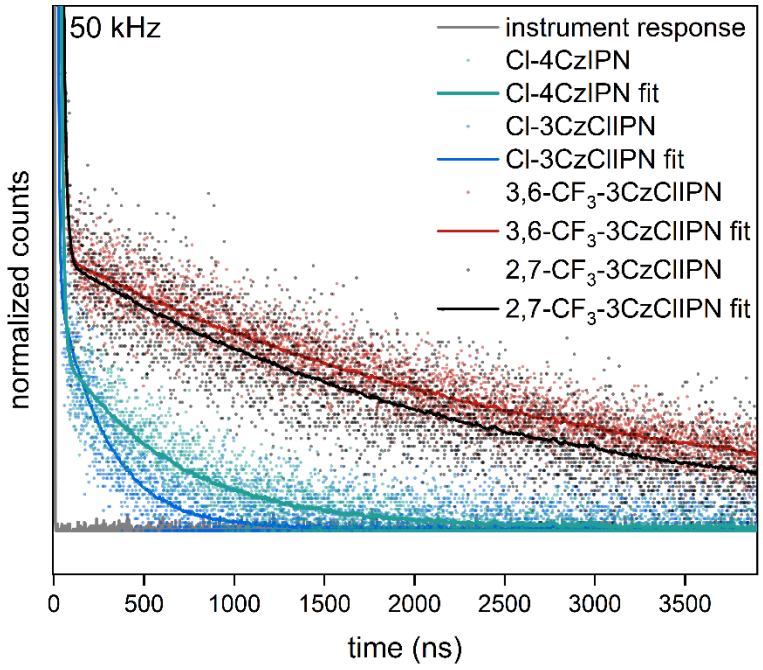

Figure S20. Vertical zoom of combined 50 kHz TCSPC decay traces (points) of Cl-4CzIPN (green), Cl-3CzClIPN (blue), 3,6-CF_3-3CzClIPN (red), and 2,7-CF_3-3CzClIPN (black) with the corresponding fit (line) and instrument response (gray line).

E. Absorbance and emission in argon compared to air

The absorbance and emission spectra for each PC were taken in argon (degassed via sparging for 30 seconds) and air to determine if there is a significant population of triplet excited states that are phosphorescing. Because oxygen is known to quench triplet states,[11] any phosphorescence would result in a change in the emission spectrum between the two samples. No significant changes in emission were observed between samples, strongly suggesting that no phosphorescence occurs at room temperature.

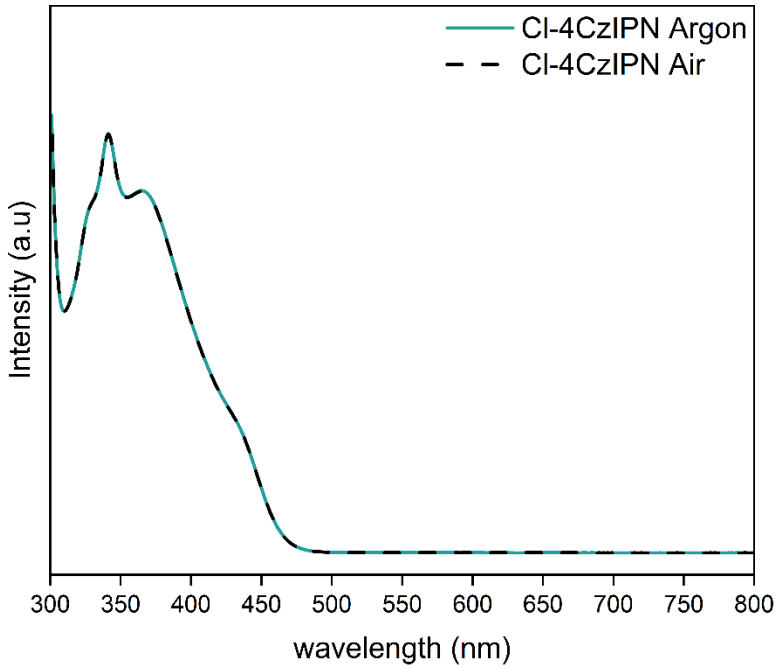

Figure S21. Normalized absorbance spectra of Cl-4CzIPN (63 µM) in argon (solid green) and in air (dashed black).

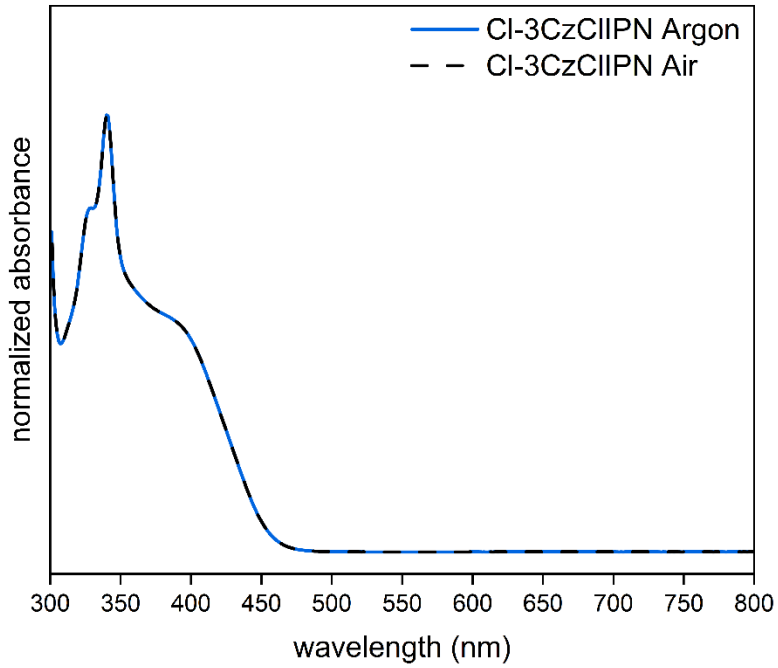

Figure S22. Normalized absorbance spectra of Cl-3CzClIPN (3.14x dilution from saturated) in argon (solid blue) and in air (dashed black).

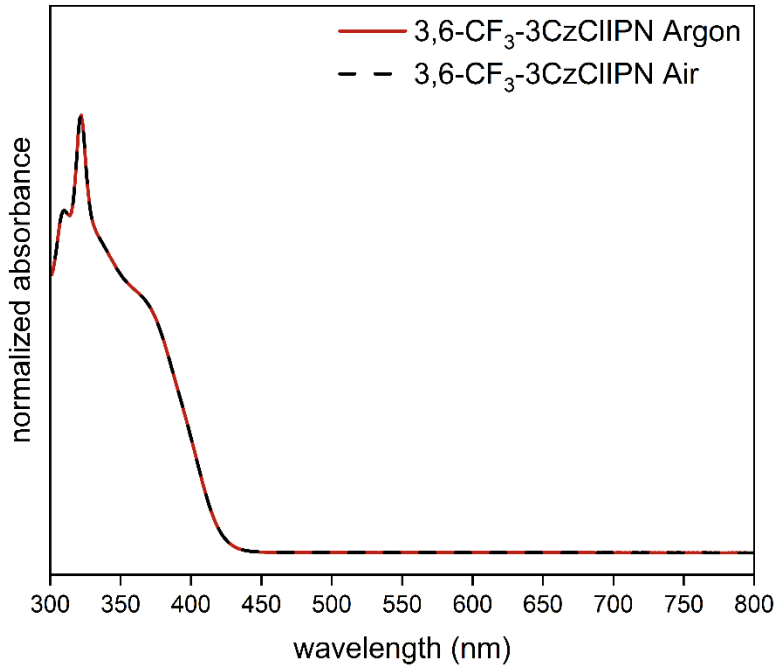

Figure S23. Normalized absorbance spectra of 3,6-CF_3-3CzClIPN (53 µM) in argon (solid red) and in air (dashed black).

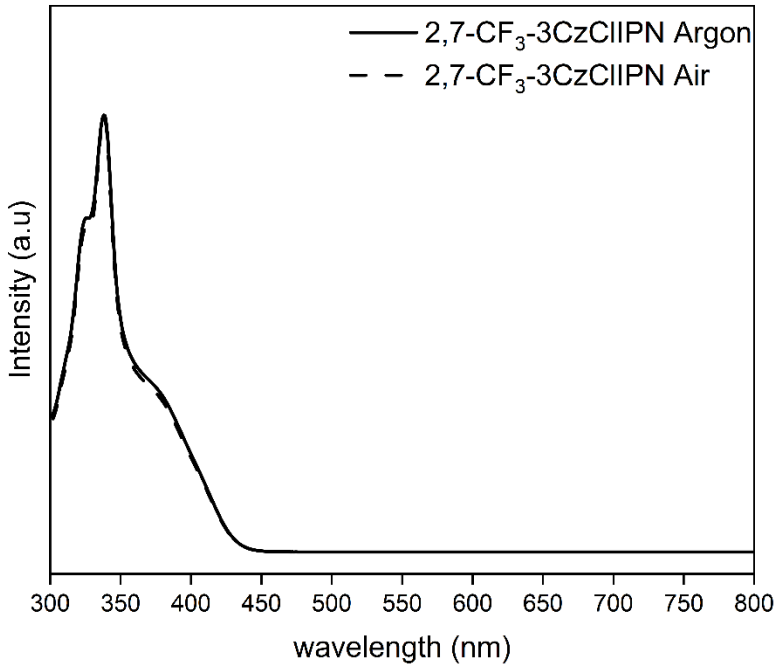

Figure S24. Normalized absorbance spectra of 2,7-CF_3-3CzClIPN (127 µM) in argon (solid black) and in air (dashed black).

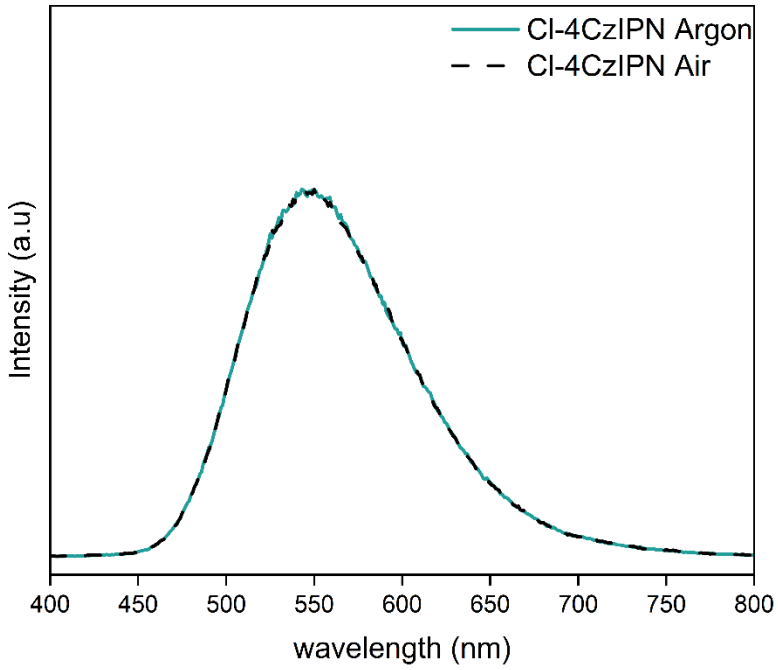

Figure S25. Normalized emission spectra of Cl-4CzIPN (63 μM) in argon (solid green) and in air (dashed black). Excitation wavelength: 375 nm.

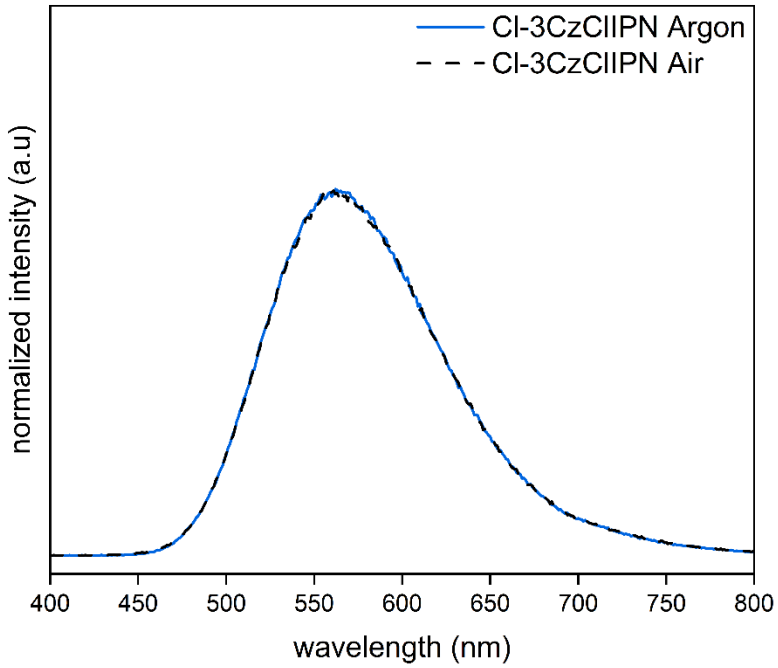

Figure S26. Normalized emission spectra of Cl-3CzClIPN (3.14x dilution from saturated) in argon (solid blue) and in air (dashed black). Excitation wavelength: 375 nm.

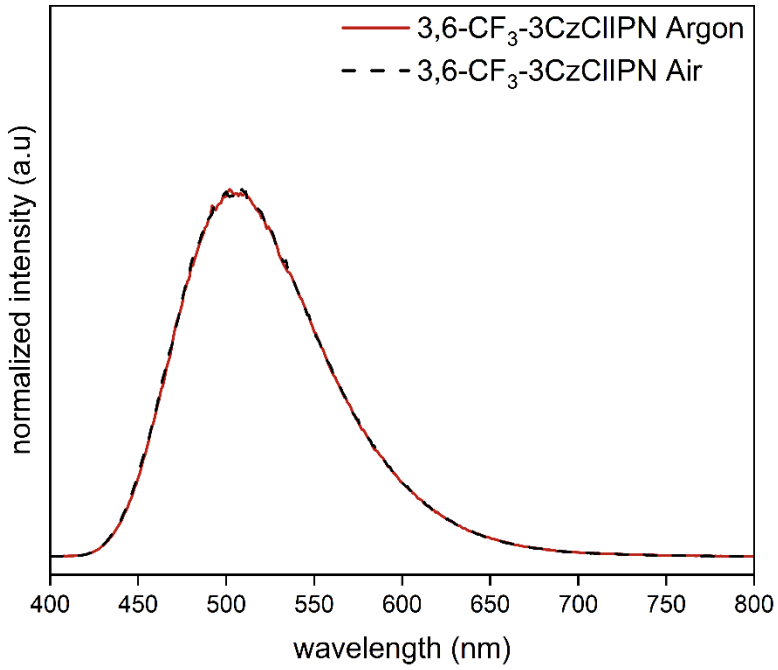

Figure S27. Normalized emission spectra of 3,6-CF_3-3CzClIPN (53 µM) in argon (solid red) and in air (dashed black). Excitation wavelength: 375 nm.

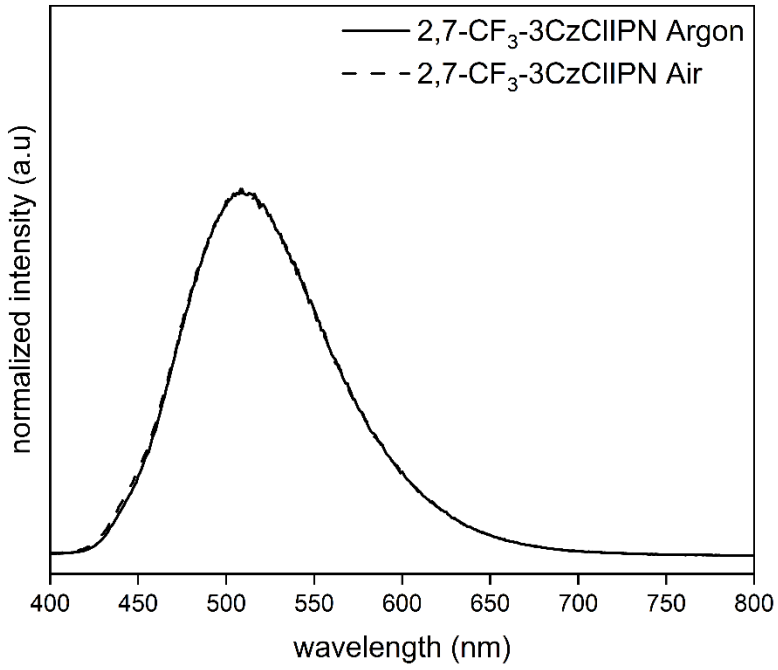

Figure S28. Normalized emission spectra of 2,7-CF_3-3CzClIPN (127 µM) in argon (solid black) and in air (dashed black). Excitation wavelength: 375 nm.

F. Cyclic voltammetry Ohmic drop investigation

CV experiments conducted in acetonitrile resulted in a 60–200 mV peak-to-peak separation (ΔE) for the PCs studied in this work. To assess whether this peak-to-peak separation accurately assessed the reversibility of the electron transfer, an Ohmic drop investigation based on the ferrocene/ferrocenium redox couple was conducted.[12,13] Ohmic drop refers to the decrease in the potential applied to the electrochemical double layer, which is characterized by a peak elongation and large peak-to-peak separation.[14,15]

In order to determine if Ohmic drop was present in the samples and was responsible for the peak elongation, a Positive Feedback R_u (PF-RU) experiment was conducted. The experiment resulted in a measured stable resistance of 208 Ω. An *iR* compensated CV was carried out with 100% compensation (Figure S29). Gratifyingly, this voltammogram showed a decreased ΔE in comparison to the 0% compensated sample (Table S3) and within the range for a reversible electron transfer.

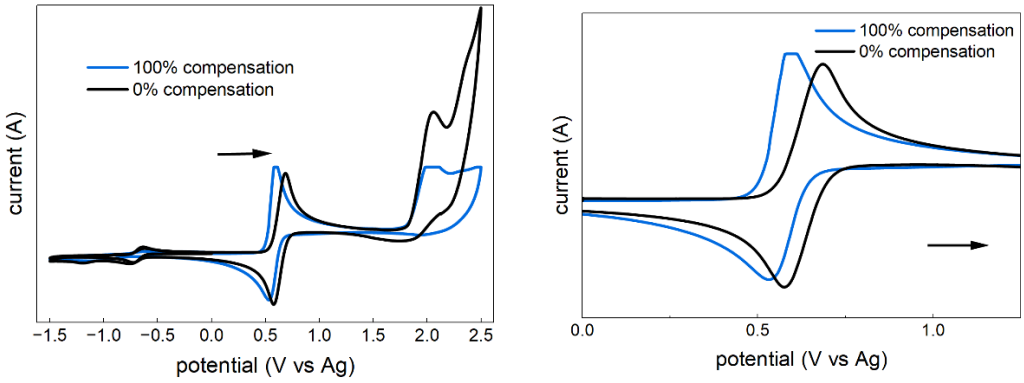

Figure S29. *iR* compensation experiment for 3,6-CF_3-3CzClIPN. 1 mM of PC with 100 mM of [BF_4^-] in acetonitrile at 100 mV/s. Potential window: −1.50 V to +2.50 V. Electrodes: glassy carbon (working), Pt (counter), Ag wire (pseudo-reference).

Table S3. *iR* compensated half–wave potential and peak-to-peak separation values for 3,6-CF_3 3CzClIPN + ferrocene

iR Compensation	$E_{1/2}$ (V)[a]	ΔE (V)[b]
100 %	0.562	0.063
0 %	0.632	0.111

Scan rate of 100 mV/s. [a] Half-wave potentials of Fc/Fc^+ redox couple. [b] peak-to-peak separation of Fc/Fc^+ redox couple.

The decrease in peak-to-peak separation of the ferrocene redox couple when resistance was compensated highlights the inherently lower conductivity of the samples. Thus, we characterized the measured $PC/PC^{\bullet-}$ redox couple as a reversible electron transfer and attribute the slight increase in peak-to-peak separation (63–78 mV) to the solution conductivity.

G. Cyclic voltammetry

1. Cl-4CzIPN

When taking CV of the redox events of Cl-4CzIPN with a potential window large enough to encompass both events, the irreversible oxidation event would cause additional reduction events near the reversible reduction, obscuring the desired event. To avoid this, the reduction (Figure S30) and oxidation (Figure S31) were measured separately.

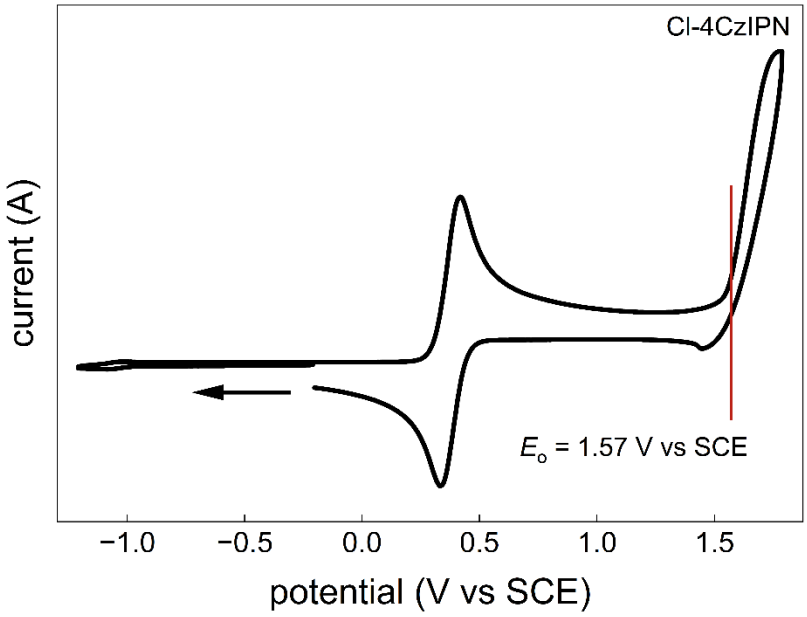

Figure S30. Cyclic voltammogram of $E_o(PC^{\bullet+}/PC)$ of Cl-4CzIPN estimated using the onset potential. The concentration of the analyte was 100 µM. Electrodes: glassy carbon (working), Pt (counter), Ag wire (pseudo-reference). The additional peak is the ferrocene redox couple.

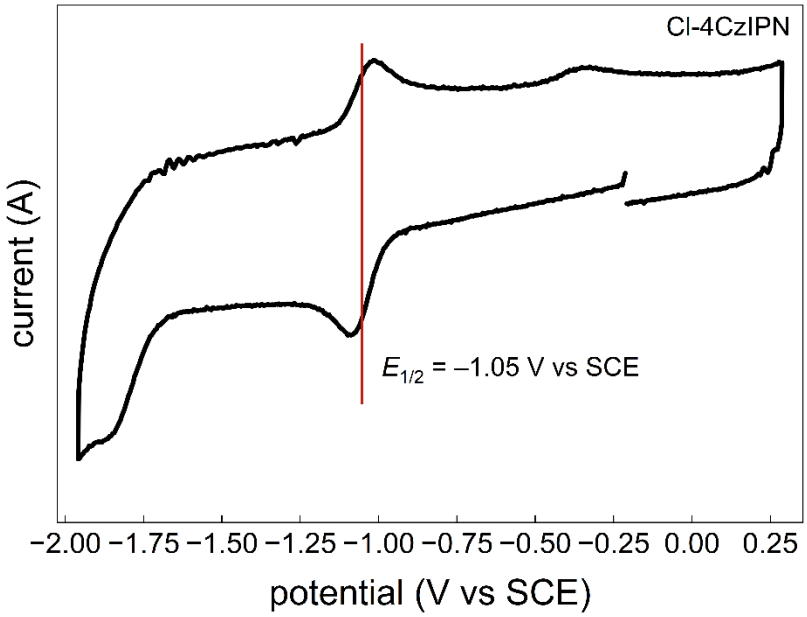

Figure S31. Cyclic voltammogram of $E_{1/2}$(PC/PC$^{\bullet-}$) of Cl-4CzIPN. The concentration of the analyte was 100 µM. Electrodes: glassy carbon (working), Pt (counter), Ag wire (pseudo-reference).

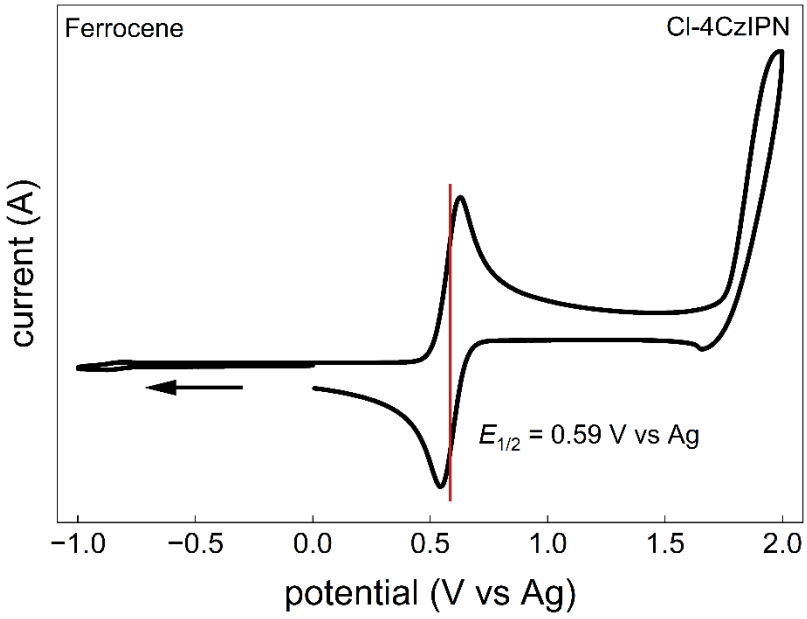

Figure S32. Cyclic voltammogram of the redox event for Ferrocene measured after analysis of Cl-4CzIPN by adding ferrocene into the analyte solution. Electrodes: glassy carbon (working), Pt (counter), Ag wire (pseudo-reference).

2. Cl-3CzClIPN

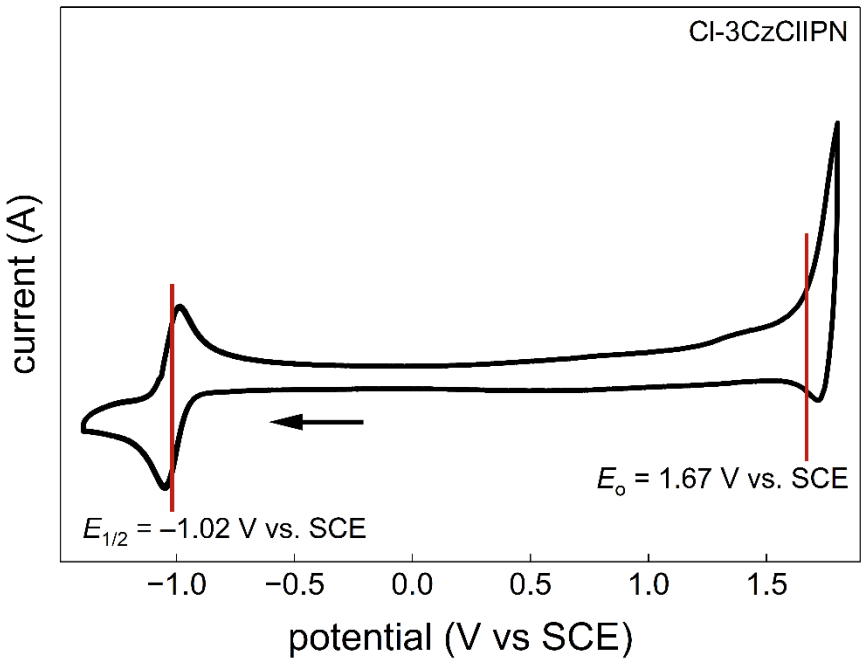

Figure S33. Cyclic voltammogram of both $E_{1/2}(PC/PC^{\bullet-})$ and $E_o(PC^{\bullet+}/PC)$ of Cl-3CzClIPN. The concentration of the analyte was 725 µM. Electrodes: glassy carbon (working), Pt (counter), Ag wire (pseudo-reference).

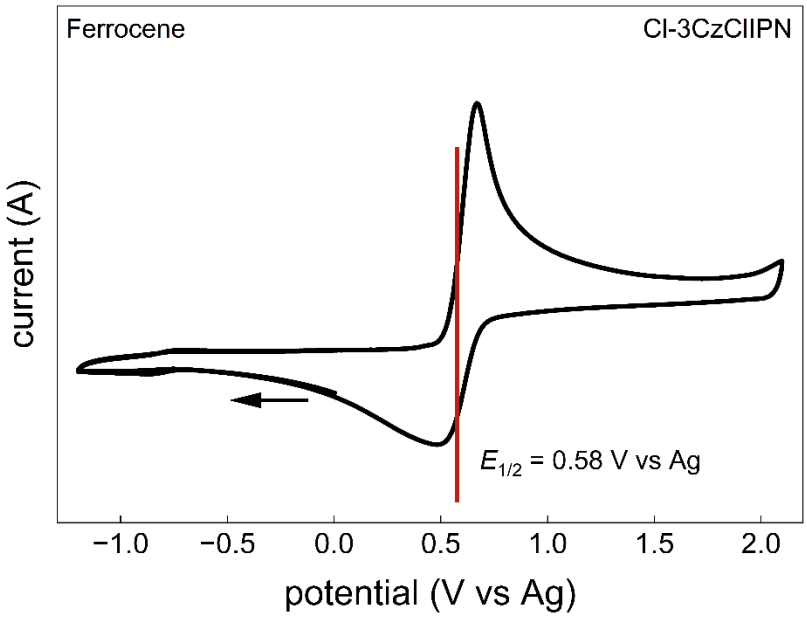

Figure S34. Cyclic voltammogram of the redox event for Ferrocene measured after analysis of Cl-3CzClIPN by adding ferrocene into the analyte solution. Electrodes: glassy carbon (working), Pt (counter), Ag wire (pseudo-reference).

3. 3,6-CF_3-3CzClIPN

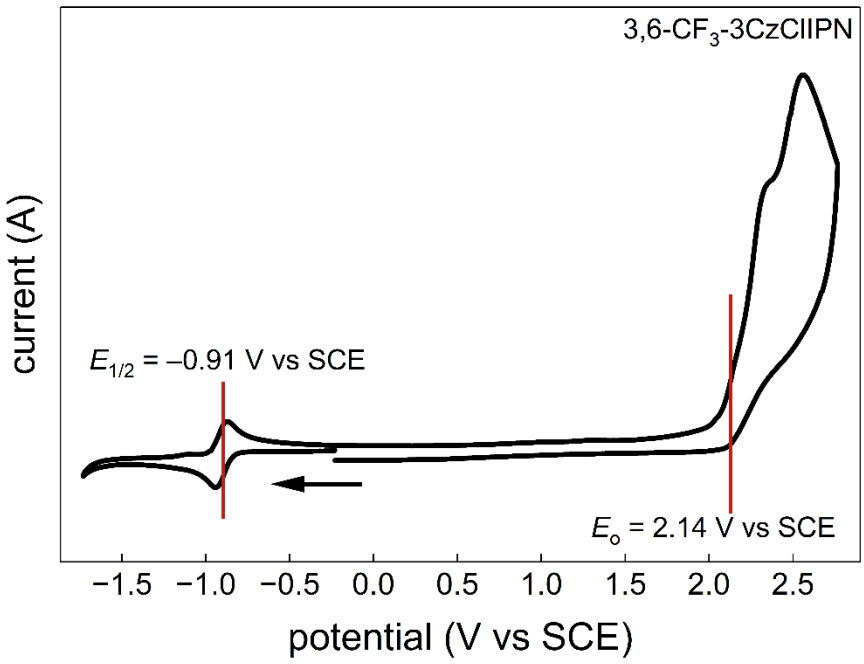

Figure S35. Cyclic voltammogram of both $E_{1/2}$(PC/PC$^{\bullet-}$) and E_o(PC$^{\bullet+}$/PC) of 3,6-CF_3-3CzClIPN. The concentration of the analyte was 242 µM. Electrodes: glassy carbon (working), Pt (counter), Ag wire (pseudo-reference).

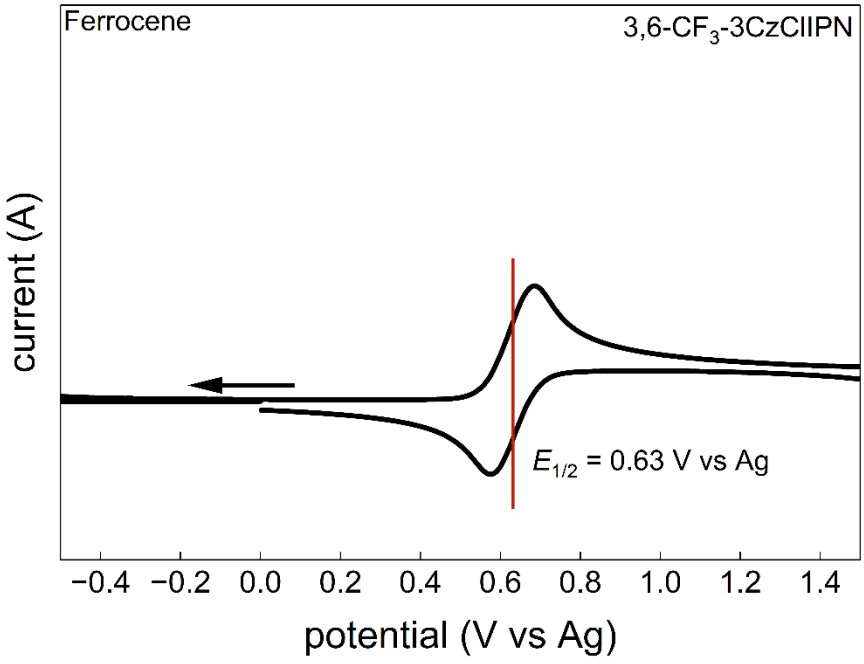

Figure S36. Cyclic voltammogram of the redox event for ferrocene measured after analysis of 3,6-CF_3-3CzClIPN by adding ferrocene into the analyte solution. Electrodes: glassy carbon (working), Pt (counter), Ag wire (pseudo-reference).

4. 2,7-CF_3-3CzClIPN

When taking CV of the redox events of 2,7-CF_3-3CzClIPN with a potential window large enough to encompass both events, the irreversible oxidation event would cause additional reduction events near the reversible reduction, obscuring the desired event. To avoid this, the reduction (Figure S37) and oxidation (Figure S38) were measured separately.

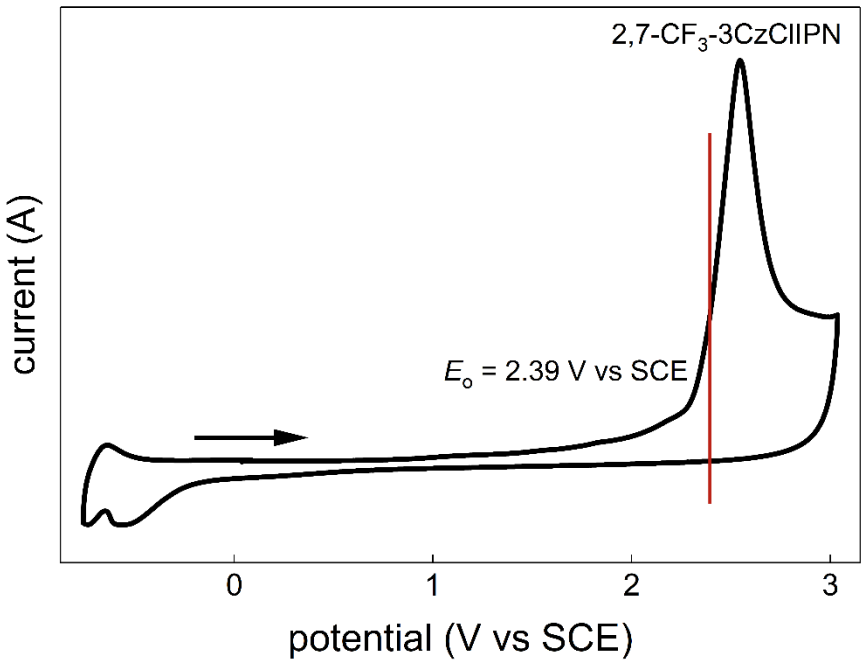

Figure S37. Cyclic voltammogram of $E_o(PC^{\bullet+}/PC)$ of 2,7-CF_3-3CzClIPN estimated using the onset potential. The concentration of the analyte was 1 mM. Electrodes: glassy carbon (working), Pt (counter), Ag wire (pseudo-reference).

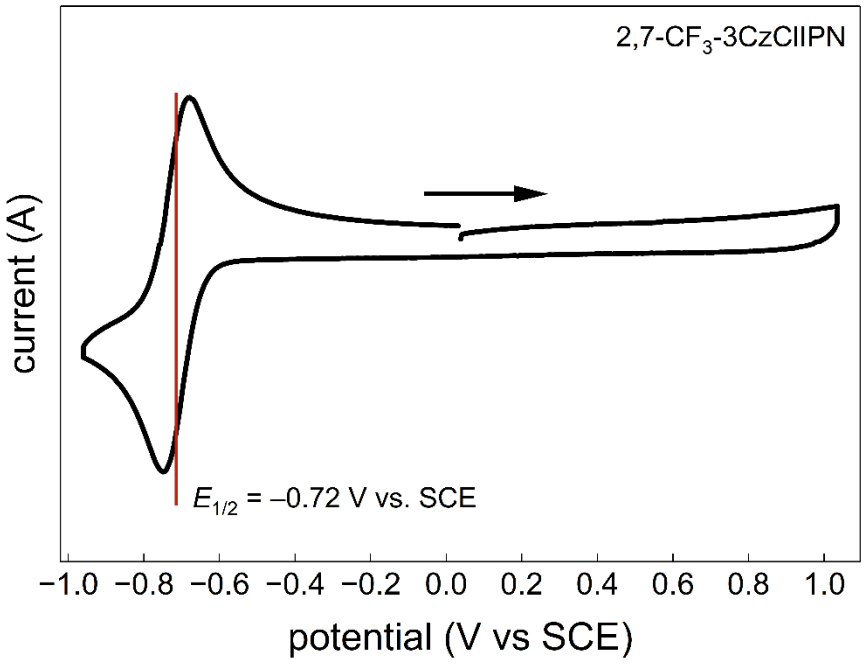

Figure S38. Cyclic voltammogram of $E_{1/2}$(PC/PC$^{\bullet-}$) of 2,7-CF_3-3CzClIPN. The concentration of the analyte was 1 mM. The potential window was adjusted to assess the reversibility of the PC/PC$^{\bullet-}$ redox couple. Electrodes: glassy carbon (working), Pt (counter), Ag wire (pseudo-reference).

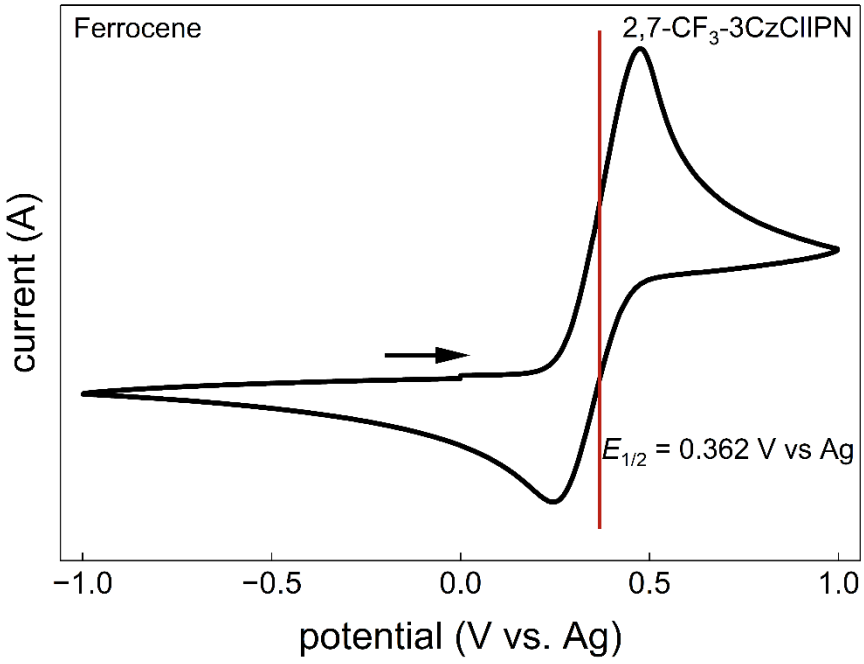

Figure S39. Cyclic voltammogram of the redox event for ferrocene measured after analysis of 2,7-CF_3-3CzClIPN by adding ferrocene into the analyte solution. Electrodes: glassy carbon (working), Pt (counter), Ag wire (pseudo-reference).

5. Discussion of the redox potentials

The previously reported redox potentials for Cl-4CzIPN[3] are outliers compared to the broader cyanoarene PC literature,[3,16] which could be due to different characterization or approximation methods. As such, we synthesized Cl-4CzIPN (see Section IV.A) and characterized it using our methods for a more consistent comparison. The ground-state reduction potentials were all fairly reversible (see Section SII.F) and are discussed in the main text. The ground-state oxidation ($PC^{\bullet+}$/PC) redox couples were irreversible for all PCs (which is commonplace for cyanoarenes[2,3,7,8,17]), and thus, the potentials were estimated using the onset potential (E_o). The effect of replacing a carbazole on the central acceptor cyanoarene ring with a chloro-group caused an increase in potential for E_o ($PC^{\bullet+}$/PC), with an increase from +1.57 V to +1.67 V for 3,6-Cl- PCs (Table S4, entries 1 and 2) and an increase from +1.68 V to +2.14 V for 3,6-CF_3- PCs (entries 3 and 4). No oxidation potential was reported for 2,7-CF_3-4CzIPN and thus could not be compared. The corresponding excited-state reduction potentials ($E_{1/2}(PC^{\bullet+}/PC^*)$ = −1.14 V to −0.47 V, entries 2, 3, 4, and 6) are fairly weak, as expected.

6. Excited-state redox potential calculations

Excited state oxidation and reduction potentials were estimated using the following formulas:

$$E_{1/2}(PC^*/PC^{\bullet-}) = E_{1/2}(PC/PC^{\bullet-}) + E_{0-0}$$

$$E_{1/2}(PC^{\bullet+}/PC^*) = E_o(PC^{\bullet+}/PC) - E_{0-0}$$

Table S4. Summary of redox potentials of PCs (reproduced Table 2 from the main text)

entry	photocatalyst	$E_{1/2}(PC/PC^{\bullet-})$ (V)[a]	$E_o(PC^{\bullet+}/PC)$ (V)[a]	E_{0-0} (eV)[c]	$E_{1/2}(PC^*/PC^{\bullet-})$ (V)[a]	$E_{1/2}(PC^{\bullet+}/PC^*)$ (V)[a]
1	Cl-4CzIPN	–1.05	+1.57	2.64	+1.59	–1.07
2	Cl-3CzClIPN	–1.02	+1.67	2.66	+1.64	–0.99
3	3,6-CF_3-4CzIPN[b]	–0.90	+1.68	2.82	+1.91	–1.14
4	3,6-CF_3-3CzClIPN	–0.91	+2.14	2.89	+1.98	–0.79
5	2,7-CF_3-4CzIPN[c]	–0.73[d]	n.d	2.81	+2.08	n.d
6	2,7-CF_3-3CzClIPN	–0.72	+2.39	2.85	+2.13	–0.47

All potentials referenced to SCE. [a] Measured using CV. [b] Literature report.[2] [c] Literature report.[8] [d] Measured using DPV. [e] Reproduced from Table 1 of the main text.

H. Storage, handling, and stability of photocatalysts

All of the PCs studied in this work were manipulated open to air over extended periods (up to 25 months in the case of 3,6-CF_3-3CzClIPN) with no degradation observed as a solid. The PCs were observed to be stable in solution (acetonitrile, hexane, acetone, ethyl acetate, and dichloromethane) up to a week in the case of a 1:4 acetone:hexane mixture, with no observable decomposition via ^{1}H NMR spectroscopy. It should be noted that no decomposition has been observed during storage of any PC – the periods outlined were the longest examples where decomposition was investigated.

The stability of cyanoarene photocatalysts to specific reaction conditions has been well-explored, such as (1) the substitution of a cyano group by a benzyl radical formed via oxidation and decarboxylation of phenylacetic acids[18,19] and (2) the substitution of the cyano group with alkyl groups by amines through β-cleavage or C–N cleavage of aminium radical cations.[20,21] These degradations lead to catalytically-productive PCs, but with altered properties from the original structures. Notably, the fluorescence is blue-shifted from yellow.

To examine the stability of the newly synthesized 3CzClIPN PCs to this kind of degradation, 2,7-CF_3-3CzClIPN was subjected to irradiation by 456 nm light for 18 hours in DMSO-d_6 in a sealed J-Young NMR tube in the presence of two sets of conditions: (1) Cs_2CO_3 and phenylacetic acid (excess rel. PC) in a N_2 atmosphere, and (2) butylamine (excess rel. PC) in a N_2 atmosphere. For both sets of conditions, we observed a complete disappearance of the original peaks in the ^{1}H NMR spectra (Figure S40 and Figure S41. These degradation peaks were also observed in the ^{1}H NMR spectra acquired after 1 hour of irradiation) and a change in fluorescence color from yellow to blue (Figure S42), indicating these PCs follow the established degradation patterns of previously studied cyanoarene PCs. While degradation occurred under these conditions, we believe these

oxidizing cyanoarene PCs can still be employed as effective catalysts based on their success with the depolymerization of phenoxy resin and the numerous reports of the 4Cz PCs being used for transformations with a variety of reactive species (nucleophiles, electrophiles, and radicals).[2,3,22]

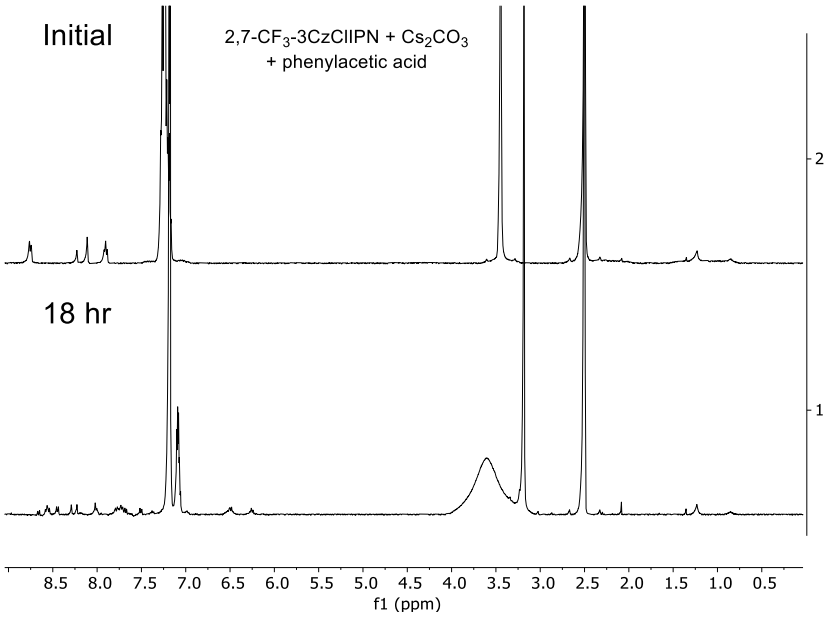

Figure S40. Stacked ^{1}H NMR spectra of initial mixture of 2,7-CF_3-3CzClIPN, Cs_2CO_3, and phenylacetic acid and following 18 hours of irradiation with 456 nm light.

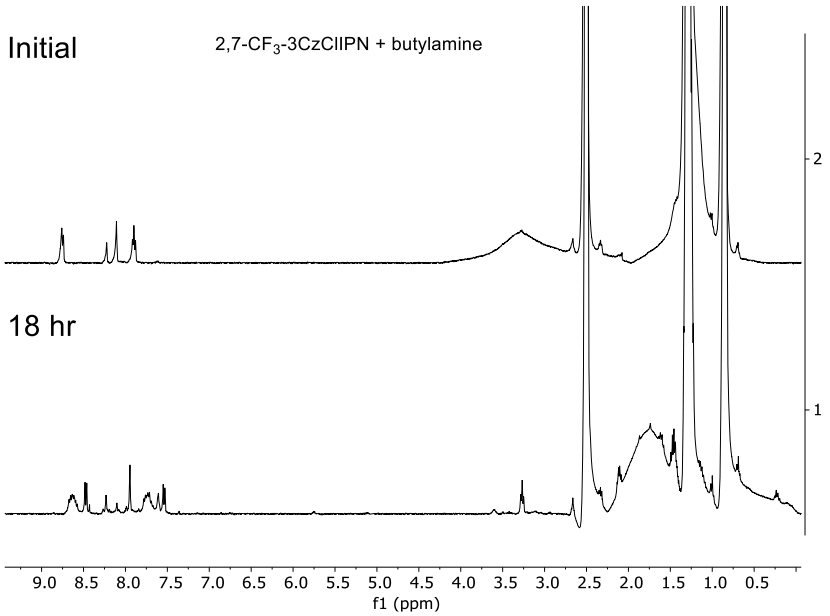

Figure S41. Stacked ^{1}H NMR spectra of initial mixture of 2,7-CF_3-3CzClIPN and butylamine and following 18 hours of irradiation with 456 nm light.

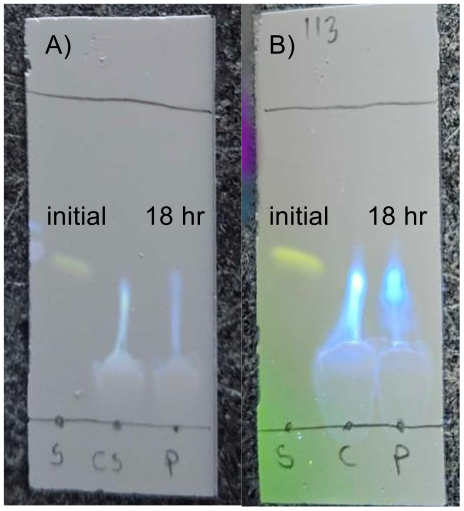

Figure S42. Thin-layer chromatography of degradation test reactions following 18 hours of irradiation with 456 nm light. (A) 2,7-CF_3-3CzClIPN, Cs_2CO_3, and phenylacetic acid. (B) 2,7-CF_3-3CzClIPN and butylamine. Run in 30% acetone in hexane as the mobile phase.

I. Calibration curve for GC analysis of depolymerizations

In order to quantify the yield of dimethoxy bisphenol A (**1**) from the depolymerization of phenoxy resin, we constructed a calibration curve of the response factor compared to the internal standard 1-bromonaphthalene (IS). To generate the calibration curve, three independent solutions of five different molar ratios of **1**:IS (1:1, 0.8:1, 0.6:1, 0.4:1, 0.2:1, 0.1:1) were prepared in THF, and each sample was measured via GC. The area of the corresponding peaks were tabulated and fitted to generate the calibration curve.

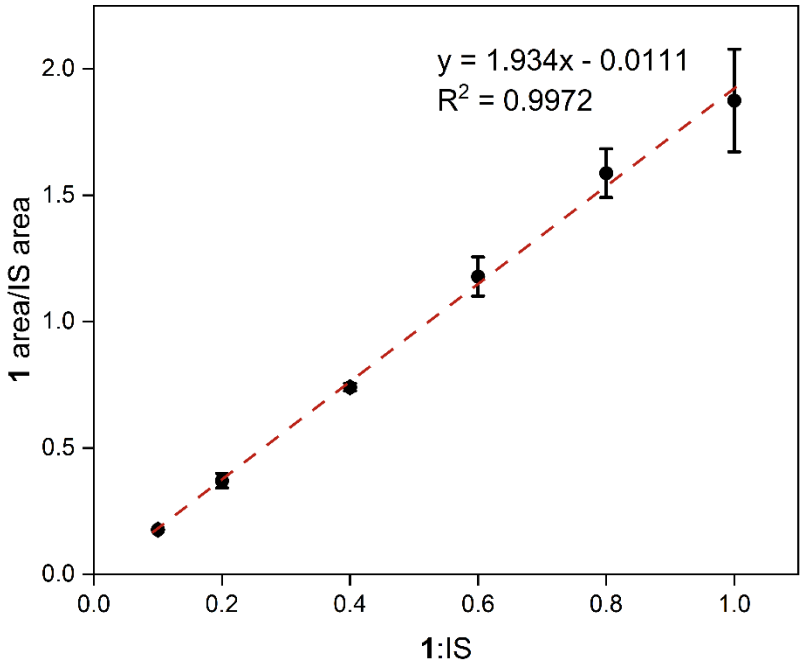

Figure S43. Calibration curve of dimethoxy bisphenol A (**1**) depolymerization product compared to internal standard 1-bromonaphthalene (IS). Error bars correspond to the standard deviation.

Table S5. Summary of GC peak areas for **1**:IS calibration curve generation.

Sample (**1**:IS)	**1** area	IS area	**1** area/IS area
1:1 A	2232011	1057157	2.111334
1:1 B	2136778	1322854	1.615279
1:1 C	2146600	1131380	1.897329
0.8:1 A	1881214	1094651	1.718551
0.8:1 B	1910515	1228885	1.554674
0.8:1 C	1812531	1217023	1.489315
0.6:1 A	1347055	1121082	1.201567
0.6:1 B	1395706	1299585	1.073963
0.6:1 C	1396530	1109095	1.259162
0.4:1 A	908055	1221905	0.743147
0.4:1 B	930631	1227911	0.757898
0.4:1 C	950554	1317414	0.72153
0.2:1 A	421051	1220591	0.344957
0.2:1 B	435567	1060263	0.41081
0.2:1 C	461191	1295782	0.355917
0.1:1 A	214947	1219393	0.176274
0.1:1 B	215094	1204763	0.178536
0.1:1 C	211421	1199761	0.176219

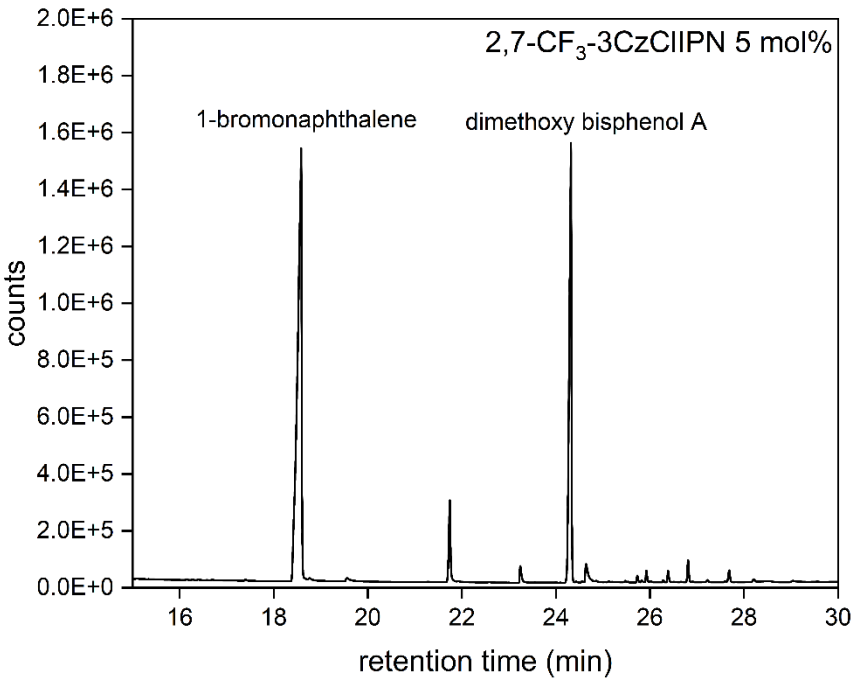

Figure S44. Representative gas chromatogram of the crude depolymerization mixture (2,7-CF_3-3CzClIPN 5 mol%) after adding in the internal standard.

Table S6. Summary of GC peak areas for depolymerization reactions.

Sample (**1**:IS)	**1** area	IS area	**1** area/IS area	mmol IS	mmol repeat units (rel. -OH)[a]	Yield (%)
3,6-CF_3-3CzClIPN (1 mol%)	475032	4292701	0.11066	0.073	0.072	6
2,7-CF_3-3CzClIPN (1 mol%)	2399173	4889944	0.490634	0.073	0.064	30
2,7-CF_3-3CzClIPN (2.5 mol%)	8161804	18823636	0.433593	0.101	0.119	20
2,7-CF_3-3CzClIPN (5 mol%)	4773031	8771067	0.544179	0.074	0.064	33
No PC	0	4098096	-	0.073	0.068	0
2,7-CF_3-3CzClIPN (1 mol%) no light	0	157820	-	0.080	0.082	0

[a] Number of moles of repeat units assuming average DP of 175.

J. Size-exclusion chromatography of depolymerizations

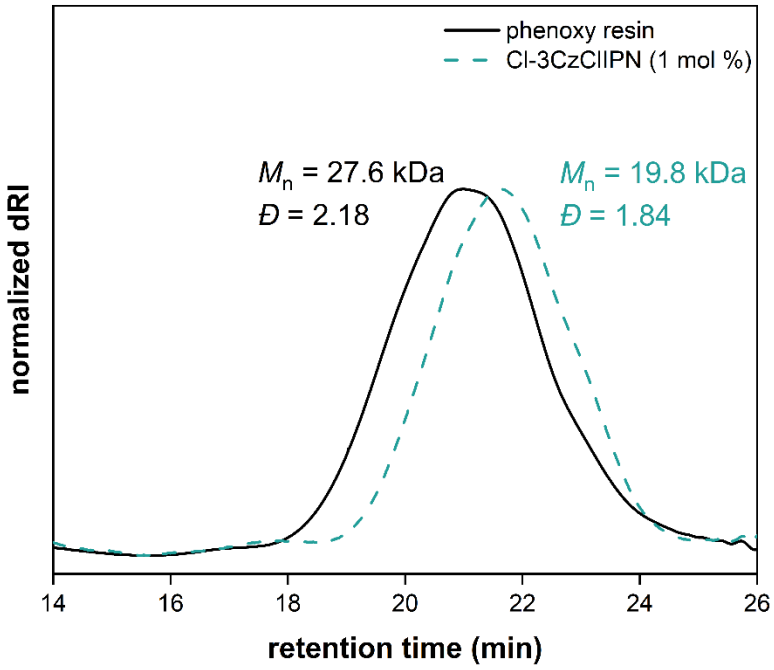

Figure S45. Size exclusion chromatogram of the depolymerization of phenoxy resin using Cl-3CzClIPN (1 mol %).

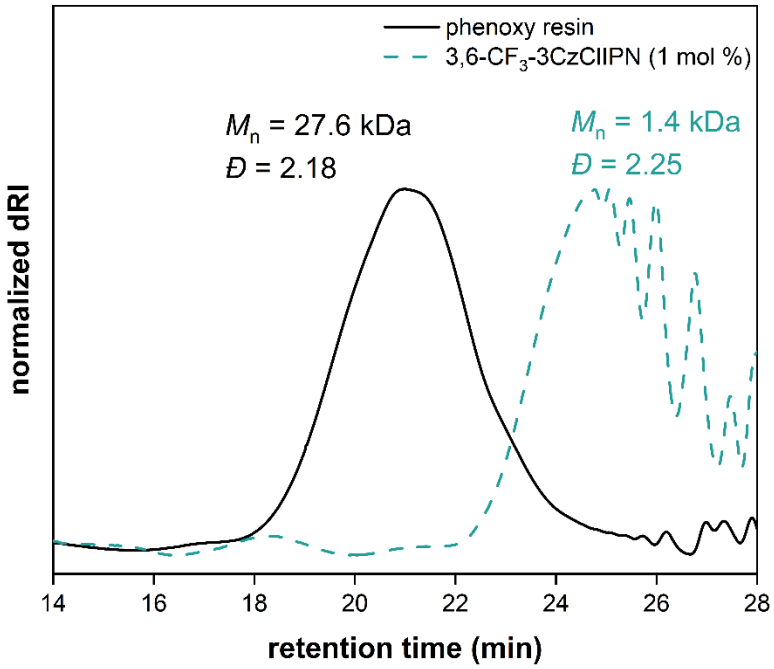

Figure S46. Size exclusion chromatogram of the depolymerization of phenoxy resin using 3,6-CF_3-3CzClIPN (1 mol %).

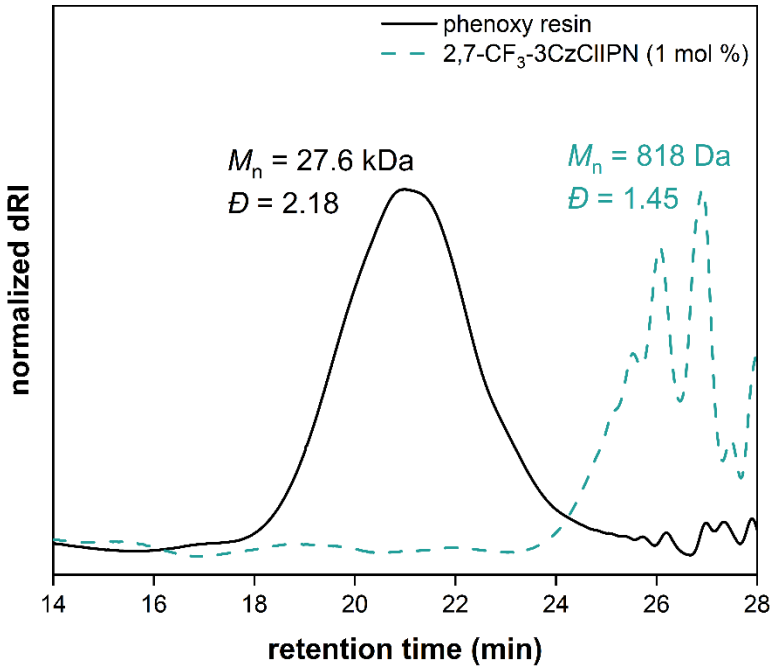

Figure S47. Size exclusion chromatogram of the depolymerization of phenoxy resin using 2,7-CF_3-3CzClIPN (1 mol %).

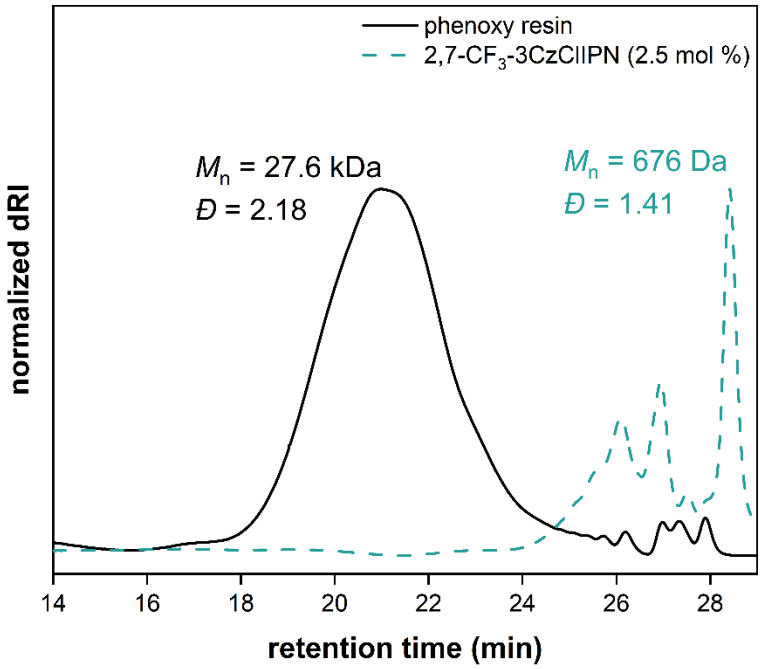

Figure S48. Size exclusion chromatogram of the depolymerization of phenoxy resin using 2,7-CF_3-3CzClIPN (2.5 mol %).

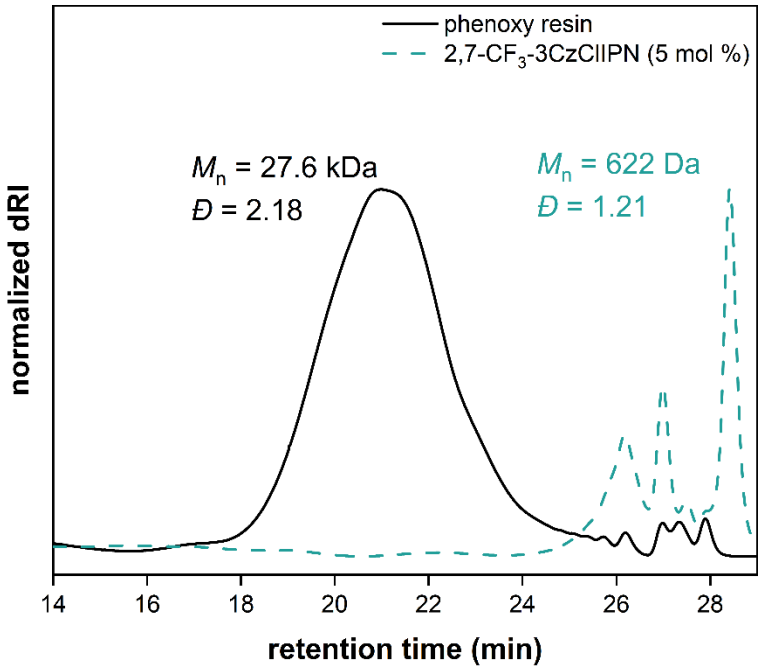

Figure S49. Size exclusion chromatogram of the depolymerization of phenoxy resin using 2,7-CF_3-3CzClIPN (5 mol %).

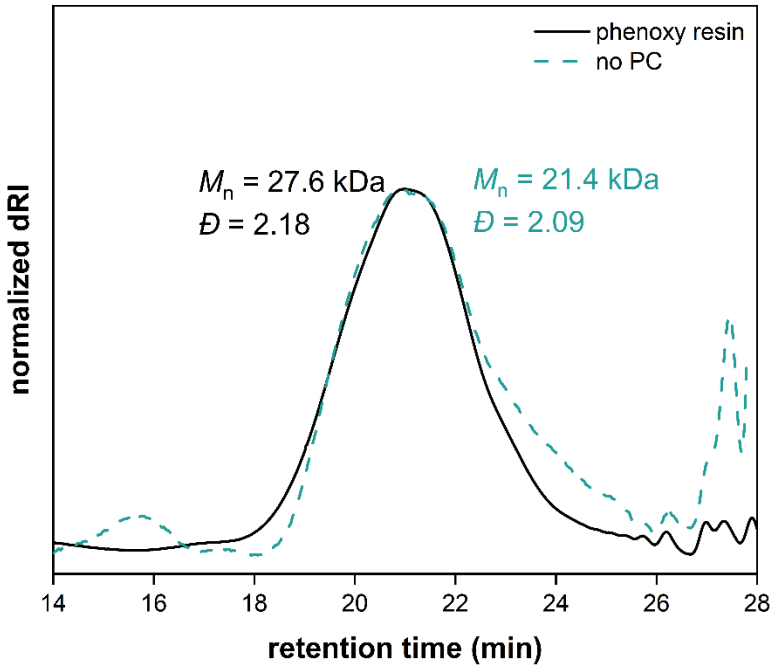

Figure S50. Size exclusion chromatogram of the depolymerization of phenoxy resin control using no PC.

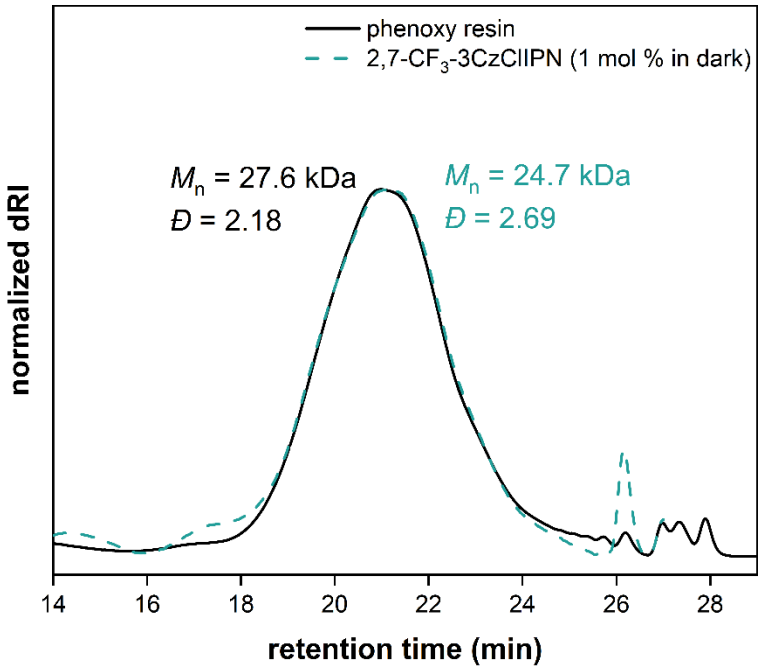

Figure S51. Size exclusion chromatogram of the depolymerization of phenoxy resin control using 2,7-CF_3-3CzClIPN (1 mol %) in the dark.

III. General synthetic procedures

A. General procedure for the depolymerization of phenoxy resin

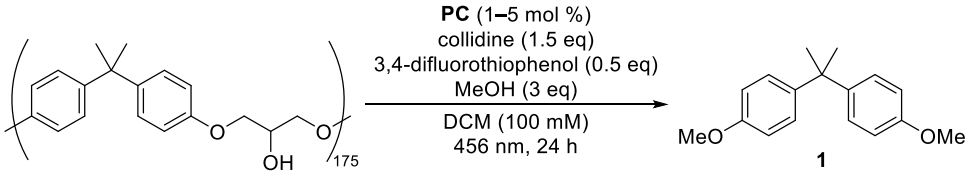

This synthesis was adapted from a previous literature procedure.[23] All equivalents were calculated with respect to the -OH group in the repeat unit of the polymer. Based on the reported molar mass of the commercial phenoxy resin (50 kDa), it was assumed the average degree of polymerization was 175. The pellet size of the commercial polymer sample was not consistent, making weighing a precise amount impractical. Therefore, the actual amount of phenoxy resin measured for each trial was used to calculate the amount of the other reagents. A representative example is described here. First, a flame-dried 1 dram vial with a septum cap was allowed to cool under active vacuum, backfilled with N_2, and equipped with a stir bar. To this vial, phenoxy resin (18.1 mg, 63 µmol in rel. -OH, 1 eq) and **PC** (3.2 µmol, 5 mol % rel. -OH) were added. The vial-cap interface was sealed using electrical tape to ensure a good seal and was carefully evacuated and refilled with N_2. Next, anhydrous DCM (636 µL, 0.1 M) was added using a 1 mL syringe, followed by collidine (2 x 5 µL (10 µL total), 76 µmol, 1.2 eq rel. -OH), 3,4-difluorothiophenol (4 µL, 32 µmol, 0.5 eq rel -OH), and anhydrous methanol (8 µL, 191 µmol, 3 eq rel. -OH) via a 10 µL gas-tight syringe. The vial was placed in the photoreactor (see Section SIII.B for details) and irradiated at 456 nm for 24 hours. Following irradiation, 1-bromonaphthalene (15.3 mg) was added

as an internal standard and allowed to stir for 5 minutes. Then, two aliquots were taken: the first was diluted with THF for GC analysis and the second was diluted in THF and filtered through a 0.2 µm PTFE syringe filter and analyzed via SEC.

B. Photoreactor setup

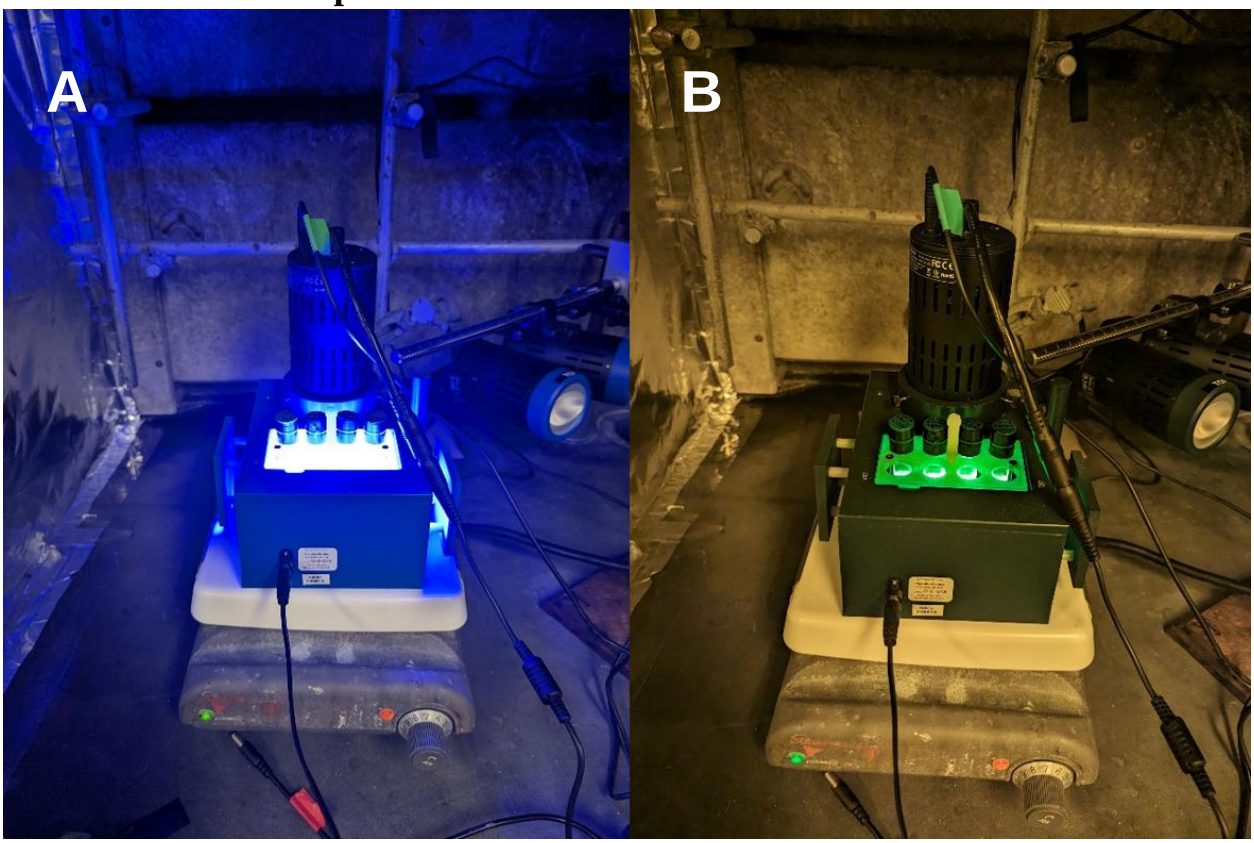

Figure S52. Images of the photoreactor setup (A) with the bulb on and (B) with the bulb on looking through HepatoChem UVEX Amber Safety Glasses.

All photochemical reactions were performed using an EvoluChem PhotoRedOx Box equipped with a single Kessil PR160L 50 W 456 nm lamp at 100% power. A Kessil lamp was chosen over the EvoluChem 18 W 450 nm LED bulbs sold with the box in order to achieve a higher light intensity. The embedded cooling fan in the box was powered, and the whole box was placed on a magnetic stirrer. This setup was placed inside of a fume hood with the sash foiled and fully closed to ensure the highest airflow and to prevent light leaking. Always be careful to wear appropriate UV- and blue-light blocking safety glasses while working with this setup.

IV. Compound synthesis and characterization

A. Cl-4CzIPN

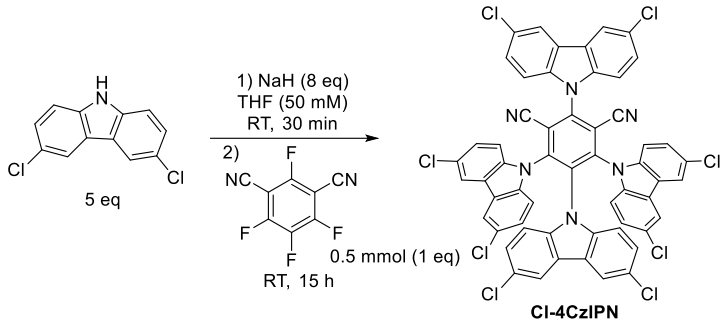

This compound was synthesized according to previous literature,[3] but was purified using a modified procedure. The crude solid was triturated with 10% acetone in hexanes and purified via column chromatography using 30% acetone in hexanes as the solvent system. NMR spectroscopy for this compound was consistent with reported values.[3]

B. Cl-3CzClIPN

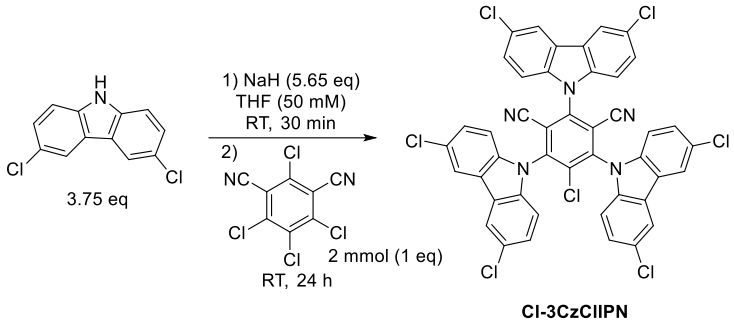

The following procedure was adapted from previous literature.[7] Inside a nitrogen-filled glovebox, sodium hydride (90%, 296 mg, 11.1 mmol, 5.64 eq) was added to a 100 mL Schlenk flask. To the flask, anhydrous THF (39.3 mL, 50 mM) was added. The flask was sealed and removed from the glovebox and cycled onto a Schlenk line. 3,6-Dichlorocarbazole (1.74 g, 7.43 mmol, 3.75 eq) was added under flow of nitrogen and allowed to stir at room temperature for 30 minutes. Then, tetrachloroisophthalonitrile (532 mg, 2.00 mmol, 1 eq) was added under flow of nitrogen. The reaction mixture was covered in foil and stirred at room temperature for 24 hours. Next, the reaction mixture was quenched via the slow addition of H_2O (20 mL). The organic layer was separated and the aqueous layer extracted with DCM (3 x 10 mL). The combined organic layer was washed with brine and dried over sodium sulfate. The solvent was removed via rotary evaporation, and the brown solid was triturated with 10% acetone in hexane to yield a bright yellow powder. The solid was purified further by flash chromatography (slow gradient from 20–30% acetone in hexane). The compound was loaded onto the column by dry loading on silica gel to yield a bright yellow solid (1.2 g, 62% yield). **^{1}H NMR** (600 MHz, acetone-d_6): δ 8.43 (s, 2H), 8.43 (s, 2H), 8.42 (s, 2H), 7.76 (d, *J* = 8.8 Hz, 2H), 7.66 (s, 1H), 7.64 (d, *J* = 2.1 Hz, 4 H), 7.63 (d, *J* = 2.1 Hz, 1H), 7.62 (d, *J* = 2.1 Hz, 3H), 7.61 (d, *J* = 2.1 Hz, 1H). **^{13}C NMR** (150 MHz, acetone-

d_6) δ 144.65, 143.89, 138.96, 138.54, 137.76, 127.69, 127.63, 127.60, 127.48, 124.75, 124.68, 121.30, 121.28, 118.55, 112.14, 111.10.

HRMS was attempted but no ionization of the target compound could be observed. MeCN and MeOH were used in various ratios and concentrations, as well as the addition of 0.1% formic acid to these solvents. Additionally, both positive and negative ionization were attempted with no success.

^{1}H NMR (600 MHz, acetone-d_6) spectrum of Cl-3CzClIPN

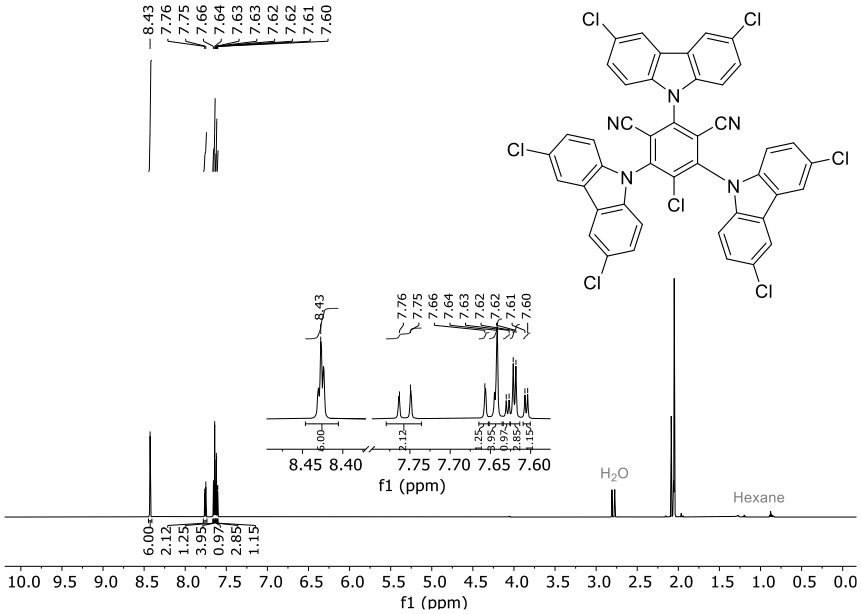

^{13}C NMR (150 MHz, acetone-d_6) spectrum of Cl-3CzClIPN

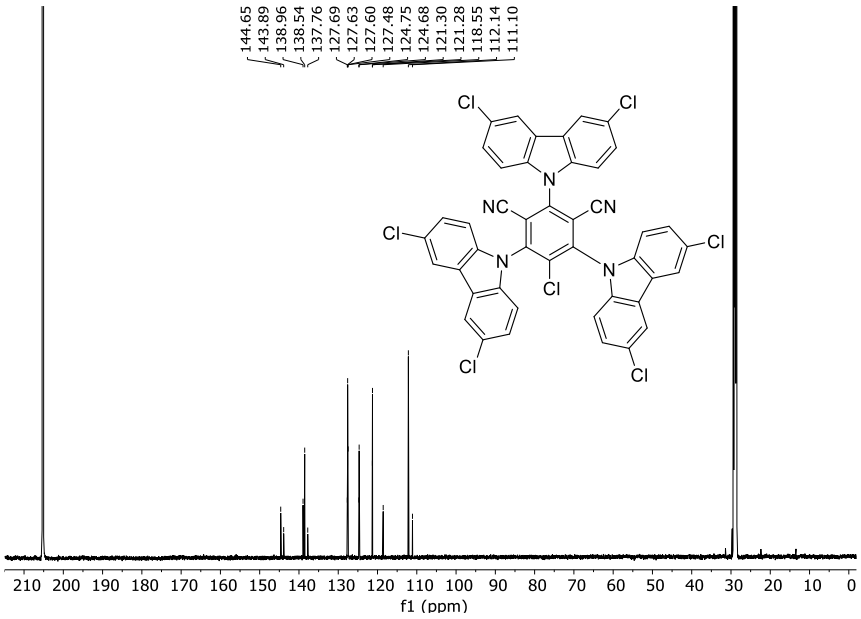

C. 3,6-CF_3-3CzClIPN

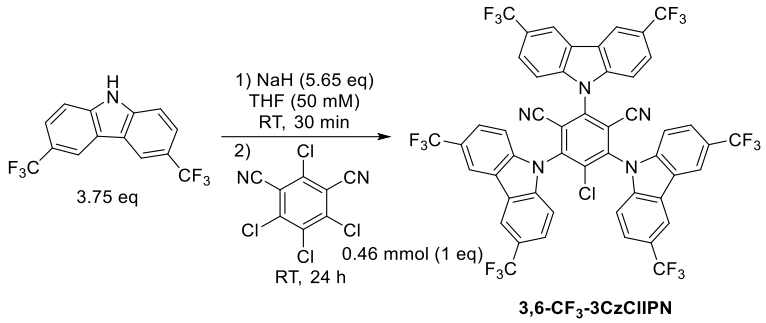

The following procedure was adapted from previous literature.[7] Inside a nitrogen-filled glovebox, sodium hydride (90%, 68.5 mg, 2.57 mmol, 5.64 eq) was added to a 50 mL Schlenk flask. To the flask, anhydrous THF (9.12 mL, 50 mM) was added. The flask was sealed and removed from the glovebox and cycled onto a Schlenk line. 3,6-Bis(trifluoromethyl)carbazole (518 mg, 1.71 mmol, 3.75 eq) was added under flow of nitrogen and allowed to stir at room temperature for 30 minutes. Then, tetrachloroisophthalonitrile (128 mg, 0.481 mmol, 1 eq) was added under flow of nitrogen. The reaction mixture was covered in foil and stirred at room temperature for 24 hours. Next, the reaction mixture was quenched via the slow addition of H_2O (10 mL). The organic layer was separated and the aqueous layer extracted with DCM (3 x 10 mL). The combined organic layer was washed with brine and dried over sodium sulfate. The solvent was removed via rotary evaporation, and the brown solid was purified via flash chromatography (slow gradient from 10–30% acetone in hexane). The compound was loaded onto the column by dry loading on silica gel. Following chromatography, the yellow powder was recrystallized in 20% acetone in hexane by first dissolving in acetone and carefully layering hexane on top to yield a yellow solid (45 mg, 43% yield). **^{1}H NMR** (600 MHz, acetone-d_6): δ 8.97 (s, 6H), 8.05 (d, *J* = 8.4 Hz, 2H), 8.01 (m, 6H), 7.94 (d, *J* = 8.6 Hz, 4H) **^{13}C NMR** (150 MHz, acetone-d_6) δ 144.34, 143.43, 142.20, 141.82, 124.90 (q, *J* = 271 Hz, 2H), 124.87 (q, *J* = 271 Hz, 4H), 124.81 (q , *J* = 3.5 Hz, 2H), 124.79 (q , *J* = 32.5 Hz, 2H), 124.78 (q, *J* = 3.6 Hz, 2H), 124.59 (q, *J* = 32.5 Hz, 4H), 138.48, 123.80, 123.74, 119.78 (q , *J* = 4.3 Hz, 4H), 119.76 (q, *J* = 4.4 Hz, 4H), 119.12, 111.66, 111.62, 110.90. **^{19}F NMR** (564 MHz, acetone-d_6) δ –61.20, –61.25.

HRMS was attempted but no ionization of the target compound could be observed. MeCN and MeOH were used in various ratios and concentrations, as well as the addition of 0.1% formic acid to these solvents. Additionally, both positive and negative ionization were attempted with no success.

^{1}H NMR (600 MHz, acetone-d_6) spectrum of 3,6-CF_3-3CzClIPN

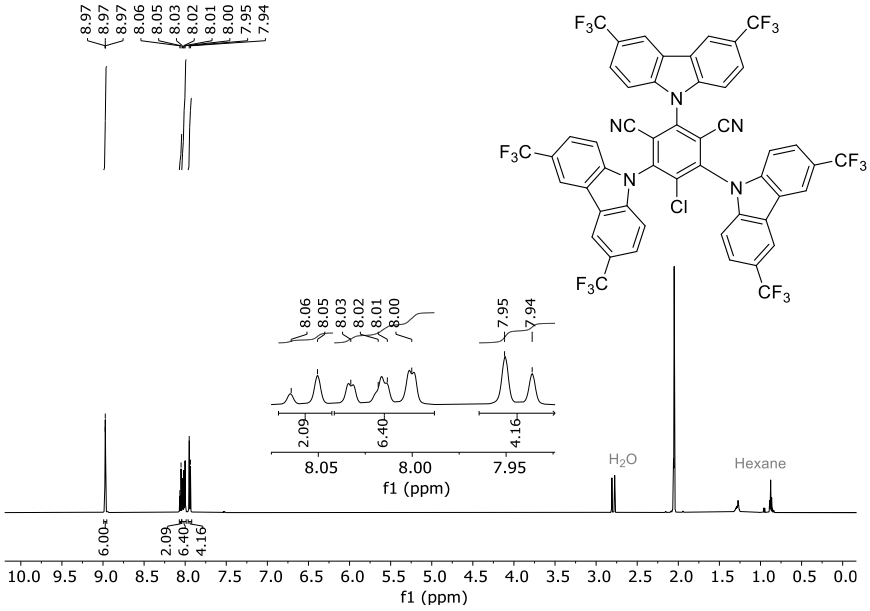

^{13}C NMR (150 MHz, acetone-d_6) spectrum of 3,6-CF_3-3CzClIPN

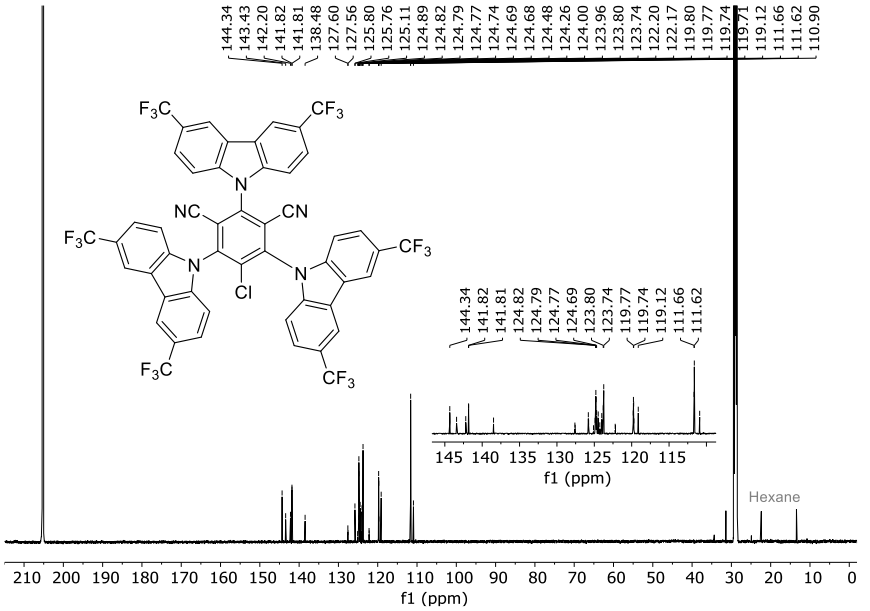

^{19}F NMR (564 MHz, acetone-d_6) spectrum of 3,6-CF_3-3CzClIPN

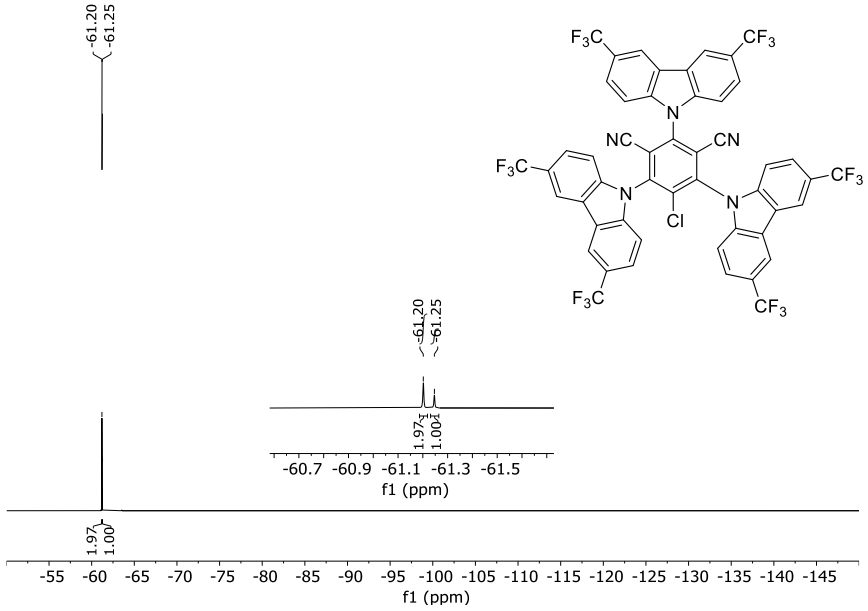

^{19}F–^{13}C HMQCGP spectrum of 3,6-CF_3-3CzClIPN to more easily identify center of quartet with J value of 271 Hz in ^{13}C spectrum.

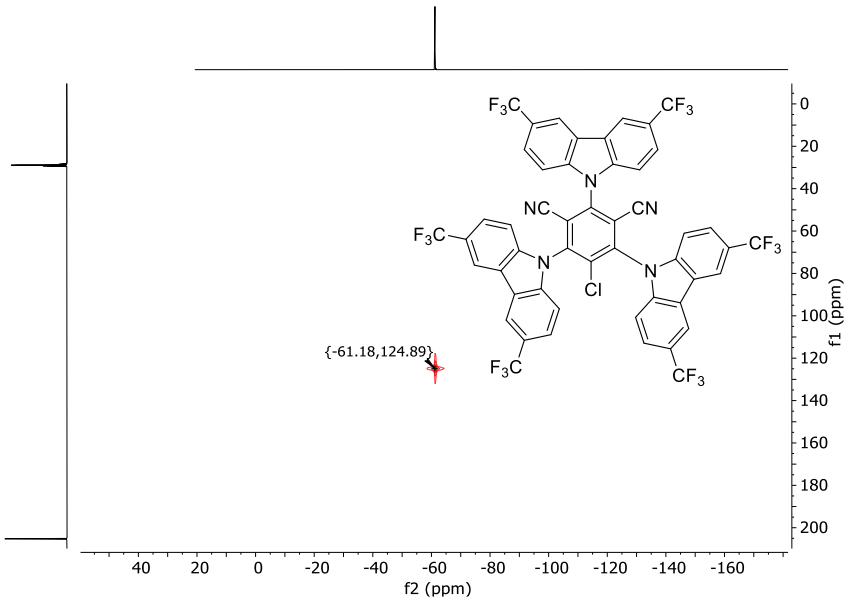

D. 2,7-CF_3-3CzClIPN

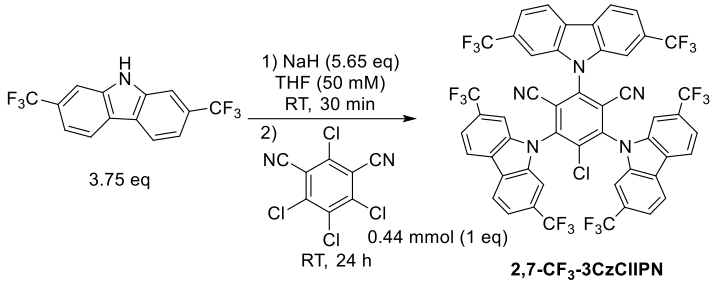

The following procedure was adapted from previous literature.[7] Inside a nitrogen-filled glovebox, sodium hydride (90%, 66.1 mg, 2.48 mmol, 5.64 eq) was added to a 50 mL Schlenk flask. To the flask, anhydrous THF (8.80 mL, 50 mM) was added. The flask was sealed and removed from the glovebox and cycled onto a Schlenk line. 2,7-Bis(trifluoromethyl)carbazole (500 mg, 1.65 mmol, 3.75 eq) was added under flow of nitrogen and allowed to stir at room temperature for 30 minutes. Then, tetrachloroisophthalonitrile (117 mg, 0.440 mmol, 1 eq) was added under flow of nitrogen. The reaction mixture was covered in foil and stirred at room temperature for 24 hours. Next, the reaction mixture was quenched via the slow addition of H_2O (10 mL). The organic layer was separated and the aqueous layer extracted with DCM (3 x 10 mL). The combined organic layer was washed with brine and dried over sodium sulfate. The solvent was removed via rotary evaporation, and the brown solid was purified via trituration with 10% acetone in hexane to yield a bright yellow powder (230 mg, 49% yield). **^{1}H NMR** (600 MHz, acetone-d_6): δ 8.73 (d, *J* = 8.6 Hz, 6H), 8.05 (s, 2H), 7.90 (m, 10H) **^{13}C NMR** (150 MHz, acetone-d_6) δ 144.35, 143.57, 140.03, 139.61, 138.09, 129.59 (q, *J* = 32.8 Hz), 129.59 (q, *J* = 32.8 Hz), 126.35, 126.29, 124.45 (q, *J* = 271.9 Hz), 124.43 (q, *J* = 171.7 Hz), 123.21, 119.71 (q, *J* = 3.7 Hz), 119.71 (q, *J* = 3.7 Hz) 119.51, 118.96, 111.07, 107.86 (q, *J* = 4.3 Hz), 107.83 (q, *J* = 4.3 Hz). **^{19}F NMR** (564 MHz, acetone-d_6) δ –61.79, –61.80.

HRMS was attempted but no ionization of the target compound could be observed. MeCN and MeOH were used in various ratios and concentrations, as well as the addition of 0.1% formic acid to these solvents. Additionally, both positive and negative ionization were attempted with no success.

^{1}H NMR (600 MHz, acetone-d_6) spectrum of 2,7-CF_3-3CzClIPN

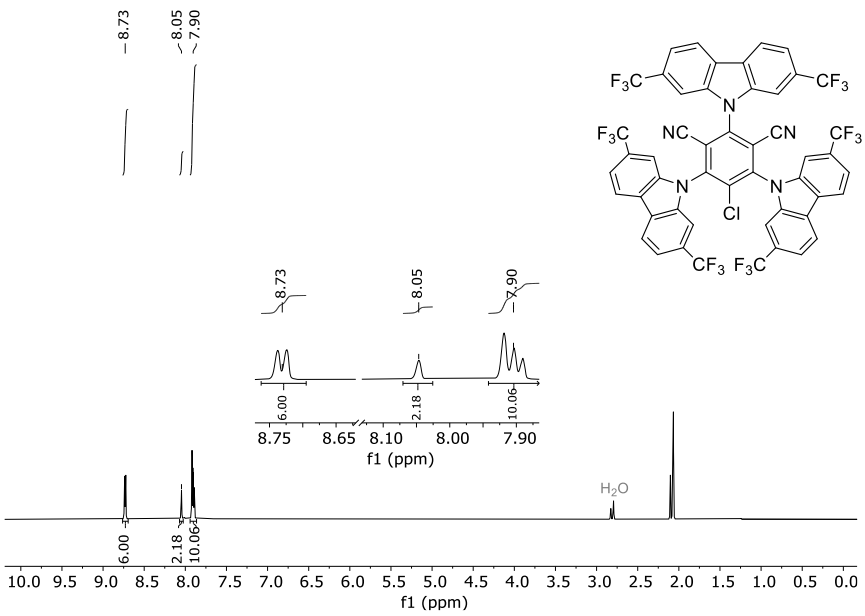

^{13}C NMR (150 MHz, acetone-d_6) spectrum of 2,7-CF_3-3CzClIPN

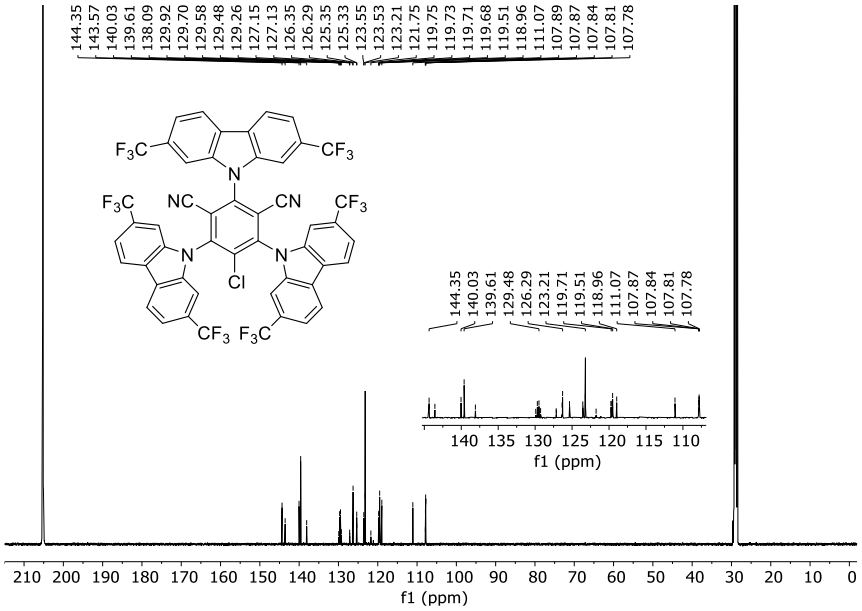

^{19}F NMR (564 MHz, acetone-d_6) spectrum of 2,7-CF_3-3CzClIPN

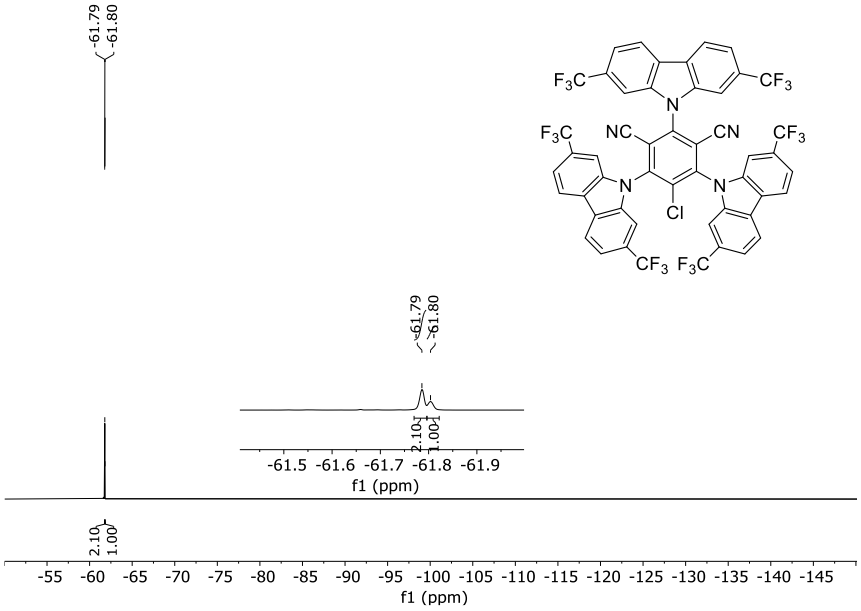

^{19}F–^{13}C HMQCGP spectrum of 2,7-CF_3-3CzClIPN to more easily identify center of quartet with J value of 272 Hz in ^{13}C spectrum.

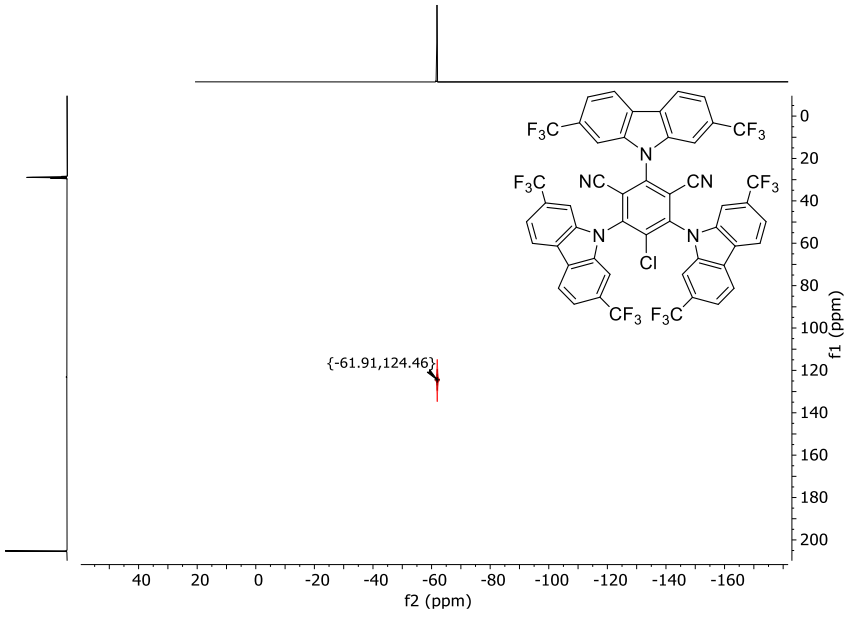

1. Crystal structure of 2,7-CF_3-3CzClIPN

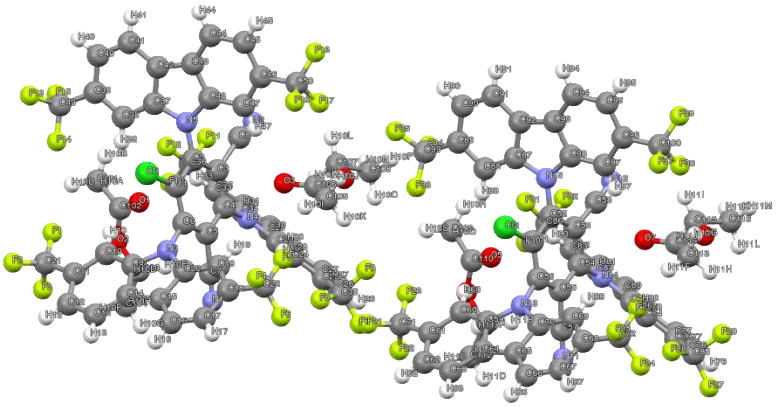

2,7-CF_3-3CzClIPN (~20 mg) was recrystallized by dissolving completely in DCM (~5 mL) before adding 4 x the volume of ethyl acetate (~20 mL) as a cosolvent. The solution was allowed to slowly evaporate to dryness over 6 days. A crystal (approximate dimensions 0.230 x 0.120 x 0.110 mm^3) was placed onto the tip of a 0.5 mm MiTeGen loop and mounted on a Bruker Photon-II CPAD diffractometer for data collection at 100(2) K. The data collection was carried out using MoKα radiation (graphite monochromator) with a frame time of 25 seconds and a detector distance of 8 cm. A strategy program was used to assure complete coverage of all unique data to a resolution of 0.80 Å. All major sections of the frames were collected with 1.2° steps in ω or ϕ at different detector positions in 2θ. The intensity data were corrected for absorption and decay (SADABS). Final cell constants were calculated from the xyz centroids of 9957 strong reflections from the actual data collection after integration (SAINT). Please refer to Table S7 for additional crystal and refinement information.

The structure was solved using SHELXT[24] and refined using SHELXL-2019/3.[25] The space group $P2_1/n$ was determined based on systematic absences and intensity statistics. A direct-methods solution was calculated which provided most non-hydrogen atoms from the E-map. Full-matrix least squares / difference Fourier cycles were performed which located the remaining non-hydrogen atoms. All non-hydrogen atoms were refined with anisotropic displacement parameters. All hydrogen atoms were placed in ideal positions and refined as riding atoms with relative isotropic displacement parameters. The final full matrix least squares refinement converged to $R1$ = 0.0562 and $wR2$ = 0.1543 (F^2, all data). A reflection (–2, 0, 2) was omitted from the final refinement due to interference from the beamstop.

Data collection and structure solution were conducted at the X-Ray Crystallographic Laboratory, S146 Kolthoff Hall, Department of Chemistry, University of Minnesota. All calculations were perform using Pentium computers using the current SHELXTL suite of programs.

Table S7. Crystal data and structure refinement for 2,7-CF_3-3CzClIPN

CCDC Number	2535799	
Empirical formula	C_{116} H_{68} Cl_2 F_{36} N_{10} O_8	
Formula weight	2484.70	
Temperature	100(2) K	
Wavelength	0.71073 Å	
Crystal system	Monoclinic	
Space group	$P2_1/n$	
Unit cell dimensions	a = 23.282(2) Å	α = 90°
	b = 17.8335(18) Å	β = 104.209(2)°
	c = 26.8489(18) Å	γ = 90°
Volume	10806.7(17) Å^3	
Z	4	
Density (calculated)	1.527 mg/m^3	
Absorption coefficient	0.187 mm^{-1}	
F(000)	5024	
Crystal color, morphology	yellow, prism	
Crystal size	0.230 x 0.120 x 0.110 mm^3	
Theta range for data collection	1.937 to 26.406°	
Index ranges	$-29 \le h \le 29$, $-22 \le k \le 22$, $-33 \le l \le 25$	
Reflections collected	125192	
Independent reflections	22166 [R(int) = 0.0549]	
Observed reflections	15344	
Completeness to theta = 25.242°	99.9%	
Absorption correction	Multi-scan	
Max. and min. transmission	0.7454 and 0.6640	
Refinement method	Full-matrix least-squares on F^2	
Data / restraints / parameters	22166 / 12 / 1631	
Goodness-of-fit on F^2	1.032	
Final R indices [I>2sigma(I)]	$R1$ = 0.0562, $wR2$ = 0.1332	
R indices (all data)	$R1$ = 0.0893, $wR2$ = 0.1543	
Extinction coefficient	n/a	
Largest diff. peak and hole	0.724 and −0.451 e.Å^{-3}	

Table S8. Atomic coordinates (x 10^4) and equivalent isotropic displacement parameters ($Å^2$ x 10^3)[a]

	x	y	z	U_{eq}
C1	7372(1)	8263(1)	2333(1)	18(1)
C2	7654(1)	7571(1)	2385(1)	19(1)
C3	7352(1)	6928(1)	2473(1)	19(1)
C4	6755(1)	6969(1)	2491(1)	20(1)
C5	6480(1)	7669(1)	2432(1)	19(1)
C6	6785(1)	8320(1)	2368(1)	18(1)
C7	5830(1)	7731(1)	2400(1)	18(1)
N1	5371(1)	7754(1)	2365(1)	36(1)
C9	6204(1)	9346(1)	1851(1)	22(1)
C10	6219(1)	9129(1)	1360(1)	26(1)
C11	5887(1)	9552(2)	958(1)	30(1)
C12	5555(1)	10177(2)	1044(1)	34(1)
C13	5550(1)	10384(2)	1535(1)	31(1)
C14	5877(1)	9967(1)	1949(1)	24(1)
C15	5968(1)	10022(1)	2497(1)	24(1)
C16	5786(1)	10530(1)	2822(1)	30(1)
C17	5974(1)	10438(2)	3345(1)	34(1)
C18	6340(1)	9837(2)	3551(1)	31(1)
C19	6534(1)	9316(1)	3242(1)	26(1)
C20	6344(1)	9424(1)	2714(1)	22(1)
C21	5872(1)	9330(2)	419(1)	42(1)
C22	6536(1)	9769(2)	4124(1)	45(1)
Cl1	7739(2)	9048(2)	2228(1)	29(1)
C8	7736(6)	6138(5)	2587(5)	18(1)
N2	7887(2)	5647(2)	2644(2)	36(1)
Cl1'	7723(4)	6108(4)	2569(4)	66(1)
C8'	7764(14)	9082(13)	2311(8)	18(1)
N2'	7892(3)	9455(4)	2084(3)	36(1)
F1	6234(2)	8784(2)	388(1)	70(1)
F2	5946(2)	9913(2)	144(1)	71(1)
F3	5321(2)	9075(2)	189(1)	67(1)
F1'	5752(6)	9819(7)	52(4)	70(1)
F2'	5566(5)	8748(5)	249(3)	71(1)

	x	y	z	U_{eq}
F3'	6441(4)	9146(6)	365(3)	67(1)
F7	5257(2)	6800(3)	4290(2)	89(1)
F8	5790(3)	7599(2)	4064(2)	96(2)
F9	6179(2)	6711(3)	4516(1)	111(2)
F7'	6229(5)	7146(9)	4369(5)	89(1)
F8'	5563(8)	6510(5)	4468(5)	96(2)
F9'	5383(6)	7461(9)	3994(4)	111(2)
O2	5751(1)	7033(1)	668(1)	40(1)
N3	6488(1)	9019(1)	2318(1)	20(1)
N4	6435(1)	6322(1)	2557(1)	22(1)
N5	8253(1)	7516(1)	2362(1)	21(1)
F4	6869(1)	10418(2)	4307(1)	66(1)
F5	6895(2)	9240(2)	4278(1)	86(2)
F6	6102(1)	9819(2)	4333(1)	66(1)
F4'	6370(4)	8970(5)	4265(3)	66(1)
F5'	6244(6)	10092(7)	4427(4)	86(2)
F6'	7061(3)	9755(8)	4360(3)	66(1)
O3	7479(1)	7133(1)	3615(1)	50(1)
O4	7523(1)	6320(1)	4258(1)	47(1)
O5	6601(1)	5801(1)	6206(1)	42(1)
O6	5801(1)	5514(1)	5579(1)	39(1)
O7	7442(1)	5502(1)	8646(1)	39(1)
O8	7473(1)	4670(1)	9274(1)	50(1)
F10	6144(1)	4617(2)	652(1)	73(1)
F11	6861(1)	4035(1)	1136(1)	71(1)
F12	6941(11)	5167(12)	950(7)	65(2)
F12'	6980(30)	5240(30)	1030(20)	65(2)
F13	8393(2)	8477(2)	291(2)	52(1)
F13'	8477(6)	8171(6)	265(6)	52(1)
F14	7593(1)	8118(1)	442(1)	52(1)
F15	8110(1)	7272(1)	208(1)	80(1)
F16	9215(2)	7977(2)	4395(1)	57(1)
F17	8909(2)	6847(2)	4307(1)	53(1)
F18	9827(2)	7043(3)	4473(2)	60(1)
F16'	9731(7)	6938(8)	4498(6)	57(1)

	x	y	z	U_{eq}
F17'	9491(4)	8020(6)	4426(4)	53(1)
F18'	8822(4)	7163(7)	4322(4)	60(1)
C23	6122(1)	6215(1)	2934(1)	24(1)
C24	6096(1)	6674(2)	3345(1)	27(1)
C25	5755(1)	6423(2)	3669(1)	31(1)
C26	5452(1)	5743(2)	3588(1)	37(1)
C27	5482(1)	5290(2)	3180(1)	35(1)
C28	5822(1)	5524(1)	2848(1)	26(1)
C29	5953(1)	5200(1)	2396(1)	25(1)
C30	5773(1)	4537(1)	2125(1)	31(1)
C31	5976(1)	4386(1)	1697(1)	31(1)
C32	6354(1)	4892(1)	1531(1)	29(1)
C33	6530(1)	5563(1)	1788(1)	24(1)
C34	6328(1)	5700(1)	2224(1)	22(1)
C35	5733(1)	6886(2)	4126(1)	40(1)
C36	6573(1)	4689(2)	1074(1)	41(1)
C37	8462(1)	7580(1)	1919(1)	22(1)
C38	8140(1)	7686(1)	1416(1)	26(1)
C39	8461(1)	7731(2)	1046(1)	29(1)
C40	9078(1)	7644(2)	1169(1)	31(1)
C41	9392(1)	7542(1)	1672(1)	28(1)
C42	9086(1)	7524(1)	2058(1)	23(1)
C43	9261(1)	7451(1)	2609(1)	23(1)
C44	9808(1)	7417(1)	2970(1)	28(1)
C45	9818(1)	7374(1)	3484(1)	30(1)
C46	9290(1)	7355(1)	3646(1)	27(1)
C47	8738(1)	7392(1)	3299(1)	25(1)
C48	8738(1)	7447(1)	2786(1)	21(1)
C49	8147(1)	7874(2)	496(1)	39(1)
C50	9318(1)	7327(2)	4205(1)	35(1)
C51	7390(1)	6791(1)	7365(1)	19(1)
C52	7664(1)	6087(1)	7435(1)	19(1)
C53	7342(1)	5456(1)	7512(1)	20(1)
C54	6739(1)	5512(1)	7501(1)	21(1)
C55	6472(1)	6218(1)	7422(1)	19(1)

	x	y	z	U_{eq}
C56	6795(1)	6859(1)	7371(1)	18(1)
C57	5824(1)	6290(1)	7364(1)	20(1)
N11	5348(1)	6318(1)	7312(1)	35(1)
C59	6205(1)	7899(1)	6864(1)	22(1)
C60	6187(1)	7678(2)	6367(1)	31(1)
Cl2	7791(1)	7575(1)	7296(1)	28(1)
C58	7609(6)	4709(9)	7617(7)	32(3)
N12	7859(2)	4173(3)	7703(2)	31(1)
Cl2'	7736(3)	4610(4)	7625(3)	34(1)
C58'	7691(8)	7455(10)	7233(7)	32(3)
N12'	7943(3)	7938(4)	7122(3)	31(1)
C61	5850(2)	8114(2)	5978(1)	41(1)
C62	5542(1)	8753(2)	6079(1)	39(1)
C63	5569(1)	8960(2)	6574(1)	32(1)
C64	5900(1)	8529(1)	6977(1)	23(1)
C65	6021(1)	8583(1)	7529(1)	23(1)
C66	5860(1)	9091(1)	7864(1)	27(1)
C67	6069(1)	8984(2)	8385(1)	30(1)
C68	6434(1)	8373(1)	8578(1)	28(1)
C69	6606(1)	7857(1)	8254(1)	23(1)
C70	6395(1)	7976(1)	7729(1)	20(1)
C71	5797(2)	7893(2)	5433(1)	72(1)
C72	6639(1)	8286(2)	9148(1)	33(1)
C73	6083(1)	4802(1)	7942(1)	23(1)
C74	6064(1)	5278(1)	8347(1)	26(1)
C75	5713(1)	5061(2)	8669(1)	29(1)
C76	5392(1)	4389(2)	8592(1)	34(1)
C77	5421(1)	3919(2)	8193(1)	32(1)
C78	5770(1)	4123(1)	7860(1)	24(1)
C79	5898(1)	3775(1)	7413(1)	24(1)
C80	5710(1)	3109(1)	7146(1)	27(1)
C81	5917(1)	2942(1)	6720(1)	28(1)
C82	6305(1)	3432(1)	6556(1)	26(1)
C83	6493(1)	4098(1)	6807(1)	23(1)
C84	6288(1)	4250(1)	7239(1)	21(1)

	x	y	z	U_{eq}
C85	5698(1)	5535(2)	9122(1)	35(1)
C86	6522(1)	3212(2)	6098(1)	37(1)
C87	8508(1)	6063(1)	7017(1)	23(1)
C88	8212(1)	6110(1)	6504(1)	24(1)
C89	8560(1)	6121(1)	6150(1)	28(1)
C90	9179(1)	6062(2)	6302(1)	30(1)
C91	9465(1)	6027(1)	6817(1)	29(1)
C92	9132(1)	6040(1)	7184(1)	24(1)
C93	9277(1)	6000(1)	7738(1)	24(1)
C94	9809(1)	5989(1)	8119(1)	29(1)
C95	9788(1)	5941(1)	8627(1)	31(1)
C96	9246(1)	5899(1)	8762(1)	28(1)
C97	8708(1)	5925(1)	8394(1)	25(1)
C98	8738(1)	5977(1)	7889(1)	23(1)
C99	8268(1)	6162(2)	5592(1)	35(1)
C100	9239(1)	5836(2)	9314(1)	37(1)
C101	6628(2)	6801(2)	422(1)	51(1)
C102	6342(1)	7064(2)	827(1)	35(1)
C103	5417(1)	7267(2)	1030(1)	39(1)
C104	4775(2)	7305(2)	735(1)	50(1)
C105	7548(2)	7597(2)	4464(1)	54(1)
C106	7512(1)	7007(2)	4064(1)	43(1)
C107	7522(2)	5692(2)	3912(1)	52(1)
C108	7311(2)	5019(2)	4142(2)	79(1)
C109	6721(1)	5269(2)	5417(1)	48(1)
C110	6385(1)	5556(2)	5782(1)	36(1)
C111	5416(1)	5776(2)	5890(1)	43(1)
C112	4795(1)	5752(2)	5559(1)	54(1)
C113	7496(2)	5935(2)	9500(1)	56(1)
C114	7468(1)	5359(2)	9093(1)	38(1)
C115	7462(2)	4068(2)	8908(1)	60(1)
C116	7373(3)	3353(3)	9171(2)	125(2)
F21	5864(2)	8450(2)	5138(1)	97(1)
F22	5254(2)	7620(2)	5216(1)	120(1)
F23	6168(2)	7354(2)	5389(1)	132(2)

	x	y	z	U_{eq}
F24	6186(1)	8176(1)	9362(1)	60(1)
F25	6922(1)	8891(1)	9373(1)	54(1)
F26	7011(1)	7714(1)	9288(1)	52(1)
F27	5171(4)	5497(5)	9263(3)	69(2)
F28	5902(2)	6264(2)	9088(2)	50(1)
F27'	5206(12)	5686(16)	9158(9)	69(2)
F28'	5652(5)	6192(7)	9004(5)	50(1)
F29	6079(1)	5304(1)	9546(1)	68(1)
F30	6089(1)	3155(1)	5675(1)	65(1)
F31	6965(2)	3668(4)	6018(3)	44(1)
F31'	6781(6)	3759(11)	5938(8)	44(1)
F32	6792(1)	2544(1)	6160(1)	57(1)
F33	7744(1)	6516(1)	5499(1)	40(1)
F34	8156(1)	5482(1)	5375(1)	50(1)
F35	8607(3)	6472(3)	5308(3)	47(1)
F35'	8565(10)	6686(10)	5379(8)	47(1)
F38	9735(1)	5561(1)	9607(1)	58(1)
O1	6598(1)	7288(1)	1249(1)	39(1)
F36	8817(1)	5368(2)	9385(1)	73(1)
F37	9143(1)	6477(1)	9517(1)	93(1)
N13	6509(1)	7567(1)	7322(1)	20(1)
N14	6404(1)	4880(1)	7566(1)	22(1)
N15	8271(1)	6019(1)	7444(1)	20(1)

[a] U_{eq} is defined as one third of the trace of the orthogonalized U_{ij} tensor.

V. References

(1) Connelly, N. G.; Geiger, W. E. Chemical Redox Agents for Organometallic Chemistry. *Chem. Rev.* **1996**, *96*, 877–910. https://doi.org/10.1021/cr940053x.

(2) Ruos, M. E.; Kinney, R. G.; Ring, O. T.; Doyle, A. G. A General Photocatalytic Strategy for Nucleophilic Amination of Primary and Secondary Benzylic C–H Bonds. *J. Am. Chem. Soc.* **2023**, *145*, 18487–18496. https://doi.org/10.1021/jacs.3c04912.

(3) Vaillant, F. L.; Garreau, M.; Nicolai, S.; Gryn'ova, G.; Corminboeuf, C.; Waser, J. Fine-Tuned Organic Photoredox Catalysts for Fragmentation-Alkynylation Cascades of Cyclic Oxime Ethers. *Chem. Sci.* **2018**, *9*, 5883–5889. https://doi.org/10.1039/C8SC01818A.

(4) Fu, B.; Dong, X.; Yu, X.; Zhang, Z.; Sun, L.; Zhu, W.; Liang, X.; Xu, H. Meso-Borneol- and Meso-Carbazole-Substituted Porphyrins: Multifunctional Chromophores with Tunable

Electronic Structures and Antitumor Activities. *New J. Chem.* **2021**, *45*, 2141–2146. https://doi.org/10.1039/D0NJ02954H.
(5) Sang, R.; Han, W.; Zhang, H.; Saunders, C. M.; Noble, A.; Aggarwal, V. K. Copper-Mediated Dehydrogenative C(Sp3)–H Borylation of Alkanes. *J. Am. Chem. Soc.* **2023**, *145*, 15207–15217. https://doi.org/10.1021/jacs.3c02185.
(6) Yokoyama, M.; Inada, K.; Tsuchiya, Y.; Nakanotani, H.; Adachi, C. Trifluoromethane Modification of Thermally Activated Delayed Fluorescence Molecules for High-Efficiency Blue Organic Light-Emitting Diodes. *Chem. Commun.* **2018**, *54*, 8261–8264. https://doi.org/10.1039/C8CC03425G.
(7) Speckmeier, E.; Fischer, T. G.; Zeitler, K. A Toolbox Approach To Construct Broadly Applicable Metal-Free Catalysts for Photoredox Chemistry: Deliberate Tuning of Redox Potentials and Importance of Halogens in Donor–Acceptor Cyanoarenes. *J. Am. Chem. Soc.* **2018**, *140*, 15353–15365. https://doi.org/10.1021/jacs.8b08933.
(8) Morofuji, T.; Kurokawa, T.; Chitose, Y.; Adachi, C.; Kano, N. Trifluoromethylated Thermally Activated Delayed Fluorescence Molecule as a Versatile Photocatalyst for Electron-Transfer- and Energy-Transfer-Driven Reactions. *Org. Biomol. Chem.* **2022**, *20*, 9600–9603. https://doi.org/10.1039/D2OB02055F.
(9) Baker, M.; Hollywood, K. A.; Hughes, C. *Biophotonics: Vibrational Spectroscopic Diagnostics*; Morgan & Claypool Publishers, 2016.
(10) Kim, H. S.; Lee, J. Y.; Shin, S.; Jeong, W.; Lee, S. H.; Kim, S.; Lee, J.; Suh, M. C.; Yoo, S. Enhancement of Reverse Intersystem Crossing in Charge-Transfer Molecule through Internal Heavy Atom Effect. *Advanced Functional Materials* **2021**, *31*, 2104646. https://doi.org/10.1002/adfm.202104646.
(11) Wilson, D. F. Oxygen Dependent Quenching of Phosphorescence: A Perspective. In *Oxygen Transport to Tissue XIV*; Erdmann, W., Bruley, D. F., Eds.; Springer US: Boston, MA, 1992; pp 195–201. https://doi.org/10.1007/978-1-4615-3428-0_20.
(12) Zheng, W. iR Compensation for Electrocatalysis Studies: Considerations and Recommendations. *ACS Energy Lett.* **2023**, *8*, 1952–1958. https://doi.org/10.1021/acsenergylett.3c00366.
(13) Heenan, A. R.; Hamonnet, J.; Marshall, A. T. Why Careful iR Compensation and Reporting of Electrode Potentials Are Critical for the CO2 Reduction Reaction. *ACS Energy Lett.* **2022**, *7*, 2357–2361. https://doi.org/10.1021/acsenergylett.2c00800.
(14) Elgrishi, N.; Rountree, K. J.; McCarthy, B. D.; Rountree, E. S.; Eisenhart, T. T.; Dempsey, J. L. A Practical Beginner's Guide to Cyclic Voltammetry. *J. Chem. Educ.* **2018**, *95*, 197–206. https://doi.org/10.1021/acs.jchemed.7b00361.
(15) Noël, T.; Cao, Y.; Laudadio, G. The Fundamentals Behind the Use of Flow Reactors in Electrochemistry. *Acc Chem Res* **2019**, *52*, 2858–2869. https://doi.org/10.1021/acs.accounts.9b00412.
(16) Ishimatsu, R.; Matsunami, S.; Kasahara, T.; Mizuno, J.; Edura, T.; Adachi, C.; Nakano, K.; Imato, T. Electrogenerated Chemiluminescence of Donor–Acceptor Molecules with Thermally Activated Delayed Fluorescence. *Angewandte Chemie International Edition* **2014**, *53*, 6993–6996. https://doi.org/10.1002/anie.201402615.
(17) Bryden, M. A.; Millward, F.; Matulaitis, T.; Chen, D.; Villa, M.; Fermi, A.; Cetin, S.; Ceroni, P.; Zysman-Colman, E. Moving Beyond Cyanoarene Thermally Activated Delayed Fluorescence Compounds as Photocatalysts: An Assessment of the Performance of a

Pyrimidyl Sulfone Photocatalyst in Comparison to 4CzIPN. *J. Org. Chem.* **2023**, *88*, 6364–6373. https://doi.org/10.1021/acs.joc.2c01137.
(18) Donabauer, K.; Maity, M.; Berger, A. L.; Huff, G. S.; Crespi, S.; König, B. Photocatalytic Carbanion Generation – Benzylation of Aliphatic Aldehydes to Secondary Alcohols. *Chem. Sci.* **2019**, *10*, 5162–5166. https://doi.org/10.1039/C9SC01356C.
(19) Grotjahn, S.; König, B. Photosubstitution in Dicyanobenzene-Based Photocatalysts. *Org. Lett.* **2021**, *23*, 3146–3150. https://doi.org/10.1021/acs.orglett.1c00836.
(20) Min, H.; Kwon, Y.; Shin, S.; Choi, M.; Mehra, M. K.; Jeon, W.; Kwon, M. S.; Lee, C. W. Tailoring the Degradation of Cyanoarene-Based Photocatalysts for Enhanced Visible-Light-Driven Halogen Atom Transfer. *Angewandte Chemie International Edition* **2024**, *63*, e202406880. https://doi.org/10.1002/anie.202406880.
(21) Kwon, Y.; Lee, J.; Noh, Y.; Kim, D.; Lee, Y.; Yu, C.; Roldao, J. C.; Feng, S.; Gierschner, J.; Wannemacher, R.; Kwon, M. S. Formation and Degradation of Strongly Reducing Cyanoarene-Based Radical Anions towards Efficient Radical Anion-Mediated Photoredox Catalysis. *Nat Commun* **2023**, *14*, 92. https://doi.org/10.1038/s41467-022-35774-5.
(22) Morofuji, T.; Kurokawa, T.; Chitose, Y.; Adachi, C.; Kano, N. Trifluoromethylated Thermally Activated Delayed Fluorescence Molecule as a Versatile Photocatalyst for Electron-Transfer- and Energy-Transfer-Driven Reactions. *Org. Biomol. Chem.* **2022**, *20*, 9600–9603. https://doi.org/10.1039/D2OB02055F.
(23) Nguyen, S. T.; McLoughlin, E. A.; Cox, J. H.; Fors, B. P.; Knowles, R. R. Depolymerization of Hydroxylated Polymers via Light-Driven C–C Bond Cleavage. *J. Am. Chem. Soc.* **2021**, *143*, 12268–12277. https://doi.org/10.1021/jacs.1c05330.
(24) Sheldrick, G. M. *SHELXT* – Integrated Space-Group and Crystal-Structure Determination. *Acta Crystallogr., Sect. A:Found. Adv.* **2015**, *71*, 3–8. https://doi.org/10.1107/S2053273314026370.
(25) Sheldrick, G. M. Crystal Structure Refinement with *SHELXL*. *Acta Crystallogr., Sect. C:Struct. Chem.* **2015**, *71*, 3–8. https://doi.org/10.1107/S2053229614024218.